University of Genoa

Master's Program in Bioengineering

Thesis submitted in partial fulfillment of the requirements for the title of Master of Bioengineering

Computing Inter-muscular Coherence During Functional Reaching Task

Yalda Salyani

March 2026

Thesis advisors:	Prof.	Michela Chiappalone
	Dr.	Marianna Semprini
Thesis co-advisors:	Dr.	Florencia Garro
	Ing.	Indya Ceroni

Contents

Abstract

Intermuscular coherence (IMC) measures the synchronization of muscle pairs, reflecting neural coordination during movement. Research on how robotic devices affect these patterns is still limited, especially regarding human-robot interaction. In this study, the FLOAT upper-limb exoskeleton developed by the Italian Institute of Technology (IIT, Genoa) was utilized to investigate changes in intermuscular coherence (IMC) during assisted and unassisted reaching tasks. Twenty healthy participants (mean age: 31±6 years; 10 females, 10 males) completed reaching tasks toward nine targets under three experimental conditions: unassisted movement, low-level robotic assistance, and high-level robotic assistance. EMG recordings were obtained from 16 upper-limb muscles during task execution. The study aimed to quantify the modulation patterns of IMC and determine how different magnitudes of assistance affect the values of intermuscular coherence. Beta-band IMC was calculated between six agonist-antagonist muscle pairs using spectral analysis techniques. Non-parametric statistical analyses were applied, including Friedman tests and Wilcoxon signed-rank post-hoc comparisons, due to non-normal data distributions, with multiple comparison correction performed using the false discovery rate (FDR) method. Robotic assistance resulted in

significant reductions in IMC across all examined muscle pairs compared to unassisted conditions. Both low and high assistance levels produced equivalent effects, with no statistically significant differences detected between them. This consistent pattern observed among participants and across targets suggests that the presence of assistance, rather than its magnitude, may determine changes in neural coordination.

Among the examined muscle pairs, Pectoralis Major and Posterior Deltoid, Middle Trapezius and Pectoralis Major, and Biceps and Triceps exhibited the greatest reductions in IMC across all targets. Moderate effects were observed in Anterior Deltoid and Posterior Deltoid, and Upper Trapezius and Lower Trapezius, while Biceps and Extensor Carpi Ulnaris demonstrated the smallest changes.

These results indicate that even minimal assistance can induce substantial coordination changes, suggesting that the mere presence of robotic support, rather than its intensity, drives alterations in neuromuscular control patterns. Understanding these effects is important for improving therapy and fostering motor recovery in rehabilitation.

Chapter 1

Introduction

1.1 Upper Limb Motor Control and Coordination

The human upper limb represents a remarkable achievement of evolutionary engineering, enabling intricate manipulation tasks that define much of human capability and independence. This sophisticated neuromuscular system facilitates countless daily activities, from basic self-care tasks to complex professional and recreational pursuits that require precise hand-eye coordination and fine motor control. However, this complex system becomes profoundly vulnerable when neurological injury disrupts its delicate coordination mechanisms, revealing the complex interdependencies that underlie seemingly effortless movements.

Stroke is a major threat to functional independence. It is the second leading cause of disability worldwide. Each year, stroke claims 6.55 million lives

and affects 101 million individuals globally [GBD 2019 Stroke Collaborators, 2021]. The impact goes far beyond numbers. Strokes can change the lives of patients and their families, affecting entire communities and healthcare systems. The demographic projections compound this challenge, with elderly populations—those most vulnerable to stroke—expected to reach 12% of the global population by 2030 and 16% by 2050 [United Nations Department of Economic and Social Affairs, Population Division, 2022]. The combination of an aging population and the doubling of stroke incidence every decade after age 55 [Norrving et al., 2018], underscores the growing importance of addressing upper limb motor control deficits within global healthcare systems.

The cascade of impairment following stroke reveals the complicated dependencies underlying upper limb function. Motor deficits progressively undermine patients' independence by reducing mobility, restricting daily activities, limiting social engagement, and precluding employment opportunities [Hatem et al., 2016]. This functional deterioration presents a significant challenge: although medical advances have improved stroke survival rates, survivors often experience long-term disabilities that persist for years after the initial injury [Carod-Artal et al., 2005]. Eighty-five percent of stroke patients experience upper limb impairment at onset. Persistent dysfunction remains in 55 to 75 percent of patients three months after stroke [Thorngren and Westling, 1990]. More than 63% of stroke survivors experience mild to severe motor and cognitive disabilities [Crichton et al., 2016]. Additionally, 30–36% are unable to ambulate without the use of assistive devices [Kelly-Hayes et al., 2003], [Jørgensen et al., 1995]. These impairments compromise

independent mobility, restrict community participation and social integration, and often result in secondary health complications [Winstein et al., 2016].

1.1.1 Neural Mechanisms of Motor Control

Neural control of upper limb movements is characterized by sophisticated interactions across distinct levels of the nervous system. This organization forms a hierarchical and integrated control structure extending from cortical planning regions to peripheral muscle fibers. At the highest level, cortical motor areas, including the primary motor cortex (M1), premotor cortex, and supplementary motor area, collaborate in the planning, initiation, and execution of voluntary movements. The primary motor cortex provides direct descending commands through corticospinal pathways, while premotor areas contribute to movement planning, preparation, and coordinating actions across multiple body segments. These descending signals are integrated at the spinal level with sensory feedback and reflex mechanisms before reaching individual muscles. This integration forms an advanced control system that enables precise coordination of voluntary movement and maintains flexibility to adapt to changing environmental conditions and specific task requirements [Reschechtko and Latash, 2018].

1.1.2 Motor Control Complexity of Reaching Movements

Reaching movements exemplify complex motor tasks that, despite appearing simple, necessitate precise coordination across multiple joints, making them essential for daily living activities [Wagner et al., 2007]. These movements demand precise coordination of multiple muscle groups at the shoulder, elbow, and wrist joints. Successful execution relies on neural control mechanisms that regulate timing, force, and spatial accuracy. Reaching is biomechanically complex due to the multiple degrees of freedom at each joint, creating what Bernstein famously termed the "degrees of freedom problem" in motor control [Wikipedia, 2024].

To perform reaching movements, the shoulder, wrist, and hand joints must be activated in a coordinated manner. Each joint contributes specific movement components that must be precisely integrated to achieve accurate target acquisition. Effective multi-joint coordination depends on advanced neural control mechanisms capable of adapting to varying target locations, movement velocities, and task requirements, while preserving both efficiency and accuracy. Hand-object interactions, which are essential for numerous daily activities, rely on coordinated reaching movements to achieve successful task completion [Valevicius et al., 2018]. Successful reaching requires extensive muscle control as well as continuous fine adjustments throughout the movement. Visual feedback directs the initial movement direction and velocity, while proprioceptive feedback allows for ongoing monitoring of limb position and movement progress. Tactile feedback is crucial during the final

phases of reaching, as contact with target objects provides information about surface properties, weight, and grip requirements.

1.1.3 Coordination Patterns in Health and After Stroke

The successful execution of reaching movements depends on the precise timing and scaling of agonist and antagonist muscle activation, which ensures smooth motion and joint stability. Agonist-antagonist coordination encompasses both the activation of prime mover muscles and the modulation of stabilizing muscles along the kinematic chain. The timing between agonist and antagonist activation influences movement speed, accuracy, and energy efficiency.

In healthy individuals, coordination patterns result from the interaction of neural control mechanisms, biomechanical constraints, and specific task objectives. The nervous system exhibits flexibility by modifying coordination strategies in response to environmental changes, target locations, and movement speeds. Such adaptability underscores the neural mechanisms that facilitate motor learning and skill acquisition throughout the lifespan.

However, neurological injury disrupts these coordination mechanisms, resulting in altered muscle activation patterns, increased co-contraction, and impaired selective muscle control. Stroke-related motor impairments weaken muscle coordination and motor function [Liu et al., 2022], creating barriers to fundamental tasks that healthy individuals perform effortlessly. The upper extremity's role in human function cannot be overstated, as musculoskeletal

damage to the arm carries exceptional clinical significance because it directly affects manual work capacity and the ability to perform activities of daily living [Park and Cho, 2017].

When neurological injury disrupts these coordination patterns, resulting in functional limitations that include social isolation, increased dependency, and reduced quality of life. The challenge of motor recovery involves not only restoring muscle strength but also reestablishing the complex coordination patterns that enable functional movement execution.

1.2 Intermuscular Coherence as a Biomarker

1.2.1 IMC Concept and Neural Basis

Efforts to understand and measure motor coordination have led researchers toward advanced electrophysiological approaches that reveal the underlying neural mechanisms of movement control. Surface electromyography provides valuable insights by recording the summed voltage potentials produced during muscle contractions using non-invasive electrodes placed on the surface of the skin [Merletti and Parker, 2004]. This technique is widely applied in neuromuscular health assessment [Zwarts et al., 2000][Yousefi and Hamilton-Wright, 2014][Hogrel, 2005], and in the development of advanced prosthetic and exoskeleton control systems [Scheme and Englehart, 2011] [Hakonen et al., 2015] [Leonardis et al., 2015] [Maciejasz et al., 2014] [Farina et al., 2014].

Neuronal synchrony analysis can be effectively performed through frequency domain techniques, which employ cross-correlation methods to ex-

amine the relationships between paired signals across time and frequency dimensions [Grosse et al., 2002]. Neural oscillations, particularly within the 15-35 Hz range, reflect the common cortical drive to muscles, providing critical insights into the functional connectivity between the brain and muscle that underlies coordinated movement [Norton, 2021]. Intermuscular coherence is a measure of functional connectivity between muscles, investigating the synchronized oscillations in electromyography signals from different muscles. Synchronization between muscles indicates that they are receiving similar neural input and operate in a coordinated manner. Neural oscillations function as a fundamental mechanism for temporal coordination across distributed neural networks, enabling precise timing of muscle activations required for smooth, coordinated movement execution.

The significance of specific frequency bands has emerged through decades of research, with the alpha (6-12 Hz), beta (13-30 Hz), and gamma bands (30-60 Hz) each providing unique insights into motor control mechanisms [Chen et al., 2018]. Alpha-band coherence has been associated with attentional and preparatory aspects of motor control, potentially reflecting sensorimotor integration processes during movement planning and execution. Additionally, alpha-band coherence is implicated in the processing of proprioceptive feedback and the integration of sensory information with motor commands. Beta-band oscillations have garnered substantial attention due to their association with corticospinal communication and voluntary motor control, providing insights into the descending control mechanisms that coordinate muscle activation patterns during voluntary movement. Gamma-band coherence appears particularly sensitive to task demands and movement dy-

namics, with higher coherence observed during dynamic tasks compared to static contractions, potentially reflecting local neural processing and fine motor adjustments.

1.2.2 IMC Analysis and Interpretation

Intermuscular coherence has evolved as a particularly sensitive biomarker for assessing coordination mechanisms, offering advantages over traditional amplitude-based electromyography (EMG) analysis by quantifying temporal synchronization between muscle groups. Coherence is calculated by analyzing EMG signals from muscle pairs to determine the degree of synchronization in their activity across specific frequency ranges. Coherence values range from 0, indicating no correlation, to 1, indicating perfect correlation. This analysis identifies common patterns between muscles while considering each muscle's individual activity level, enhancing understanding of the common neural drive that coordinates muscle activation patterns during voluntary movement. Interpretation of coherence values requires careful consideration of the physiological mechanisms underlying intermuscular synchronization. High coherence values indicate strong common neural input to the muscle pair, potentially reflecting shared cortical drive, spinal interneuronal coupling, or synchronized recruitment of motor units. Low coherence values may indicate independent control of the muscles, task-specific coordination strategies, or disrupted neural coupling resulting from pathological conditions.

1.2.3 IMC Applications and Research Findings

Jaiser and colleagues (2016) validated the clinical utility of coherence analysis by demonstrating the stability of beta-band coherence across nearly six decades of adult life. Their study of healthy adults found no significant age-related changes in coherence amplitude and identified substantial inter-individual variability that surpassed temporal variations within individuals. These results support beta-band coherence as a robust normative biomarker for corticospinal function, unaffected by age-related neural changes that may confound other measurement methods [Jaiser et al., 2016].

The clinical relevance of intermuscular coherence gained substantial support through Liu and colleagues' (2022) investigation of stroke survivors, which revealed significant alterations in coherence patterns, particularly within the alpha and gamma frequency ranges. Their findings demonstrated that stroke fundamentally reorganizes neuromuscular coordination, with the positive correlation between coherence levels in synergistic muscle pairs and motor function scores highlighting its potential as a neurophysiological biomarker for detecting and quantifying post-stroke deficits [Liu et al., 2022]. This research established coherence analysis as more than just a research tool, it emerged as a potential clinical instrument for understanding the neural basis of motor recovery.

Further evidence for the clinical utility of coherence analysis was provided by McNicol, Osuagwu, and Vučković (2025), whose investigation of task-dependent coherence revealed important insights into the factors influencing neural coordination. Their comparison between static and dynamic

hand grip tasks demonstrated significantly higher gamma-band coherence during dynamic activities, while beta-band coherence remained stable across conditions. Perhaps most intriguingly, their finding that transcutaneous electrical stimulation did not significantly alter coherence magnitudes suggested that task dynamics play a more prominent role in modulating coordination than external electrical interventions [McNicol et al., 2025]. This research highlighted the importance of considering task specificity when evaluating neural coordination, particularly relevant for applications involving assistive technologies.

1.3 Robot-Assisted Motor Rehabilitation

1.3.1 Development of Robotic Rehabilitation Systems

Recognition of the effectiveness of intensive training in promoting motor function recovery after stroke [Hatem et al., 2016] [Krakauer and Cortés, 2018] has prompted the development of technological solutions designed to address the limitations of conventional rehabilitation. Although traditional rehabilitation methods are clinically effective, they are constrained by limited therapist availability, consistency of intervention delivery, and the demanding nature of repetitive, standardized training [Krebs et al., 2014] [Balasubramanian et al., 2012] [Wright et al., 2018].

These limitations become particularly challenging when considering the growing population of stroke survivors requiring intensive rehabilitation services and the evidence suggesting that recovery outcomes improve with in-

creased training intensity and duration. Rehabilitation technology has progressed from passive mechanical devices to active robotic systems capable of providing advanced assistance and resistance during therapeutic exercises. Early rehabilitation robots were designed to deliver repetitive movement training. Systems such as MIT-MANUS [Krebs et al., 1999] pioneered the use of robotic technology for upper limb rehabilitation. These early systems demonstrated the feasibility of robotic intervention and provided initial evidence for the effectiveness of robot-assisted therapy. Recent advancements highlight the critical role of patient engagement, task-specific training, and the incorporation of neuroscientific principles into robot design and control algorithms. Modern rehabilitation robots integrate advanced sensors, complex control systems, and interactive feedback mechanisms that can adapt to individual patient needs and provide personalized therapy protocols.

1.3.2 Current State of Robotic Rehabilitation

Robotic rehabilitation technologies have emerged as promising tools for enhancing motor recovery, offering the potential for consistent, repeatable, and quantifiable assistance during therapeutic exercises. The field has experienced rapid expansion over the past decade, driven by advances in both military and medical applications of human-robot interaction systems [Wang et al., 2022]. However, developing assistive strategies that allow exoskeletons to provide efficient and natural support aligned with user intention remains a significant engineering and scientific challenge. Upper-limb exoskeletons represent advanced human-robot interaction systems designed as external structural mechanisms with joints and links that align with human body seg-

ments to facilitate rehabilitation and assistive movement [Perry et al., 2007]. These devices offer several potential advantages over conventional therapy, including the ability to provide consistent assistance levels, accurate measurement of patient performance, and standardized training protocols that can be replicated across different clinical settings and therapists. Despite more than thirty-five years of research on wearable technologies for upper-limb assistance and numerous promising preliminary results, the ultimate goal of restoring pre-impairment quality of life for individuals with physical disabilities has not yet been achieved [Proietti et al., 2022]. This gap between technological capability and clinical outcome highlights the need for a deeper understanding of how robotic assistance affects fundamental motor control mechanisms and how these effects translate into functional improvements.

1.3.3 Challenges and Research Gaps in Robotic Rehabilitation

The complexity of human-robot interaction in rehabilitation contexts extends far beyond mechanical design to encompass fundamental questions about how external assistance affects neural control mechanisms. Current understanding of these interactions remains limited, with most research focusing on functional outcomes rather than the underlying neurophysiological changes that occur during robot-assisted movement. This knowledge gap represents a significant barrier to optimizing robotic rehabilitation protocols and ensuring that technological interventions enhance rather than interfere with natural recovery processes.

The importance of establishing evidence-based approaches to robotic re-

habilitation cannot be overstated, as clinical practice relies on understanding how motor control mechanisms respond to external assistance [Levin and Piscitelli, 2022]. A well-established rehabilitation process requires ongoing assessment of patient progress and the specific impact of robotic interventions on individual rehabilitation objectives [Langhorne et al., 2011] [Oña et al., 2018]. However, current rehabilitation assessment often relies on clinical scales and functional measures that may not capture the subtle changes in neural coordination that robotic assistance might induce. One critical challenge involves determining optimal assistance strategies that promote motor learning while avoiding the development of dependency on external support. The adaptability of the nervous system suggests that repeated exposure to robotic assistance may modify coordination patterns. These modifications might be beneficial for therapy but problematic for independent function.

Recent clinical trials of robotic rehabilitation have shown variable results, emphasizing the need for a better understanding of the fundamental mechanisms through which robotic assistance affects motor control. Studying these mechanisms in healthy individuals establishes a foundation for identifying pathological changes and improving clinical interventions. This knowledge gap prevents robotic rehabilitation from reaching its full clinical potential. The present investigation addresses this gap by examining intermuscular coherence patterns during robot-assisted reaching movements, contributing to the fundamental understanding of human-robot motor interaction necessary for effective clinical translation. Understanding how external assistance—such as that provided by a wearable exoskeleton—influences IMC can help design more effective rehabilitation tools and strategies.

So far, studies have mostly focused on simple movements involving a limited number of muscles. However, performing daily activities and engaging in social interactions requires more than just simple movements such as extension and flexion. Previous studies on intermuscular coherence have predominantly examined static or isometric tasks, such as postural control, force production, or sustained muscle contractions. These studies have contributed valuable insights into the neural mechanisms underlying muscle coordination and common drive.

However, research exploring IMC during dynamic, functionally relevant movements, particularly those involving multiple joints and coordinated limb activity, remains limited. Furthermore, the influence of external assistance or rehabilitation technologies on IMC has received little attention. As a result, important aspects of how IMC reflects neuromuscular control in more naturalistic or rehabilitative contexts are still not well understood.

The main motivation of this project is to use IMC as a biomarker to quantify changes in muscle coordination during a standardized reaching task. The IMC reflects the synchronization of neural input with different muscles, providing valuable information on the functional connectivity of the motor system. Reaching is not only a representative upper-limb function but also a complex motor action involving multiple muscles and joints, making it ideal for investigating neuromuscular control. As such, reaching serves as a relevant and functionally meaningful task for evaluating motor performance in both healthy and impaired populations.

Chapter 2

Materials and Methods

2.1 Objectives of the study

The primary aim of this study is to compute intermuscular coherence (IMC) in upper limb muscles during a standardized reaching task and to assess how different assistant modes of a wearable exoskeleton influence motor coordination, as indicated by IMC. Although reaching appears to be a simple movement, it is a fundamental motor task that requires complex coordination among multiple joints and muscles.

Reaching might seem effortless, but it requires several muscles to work together to execute an action. Reaching is particularly suitable for analysing IMC because it involves the coordinated activation of multiple muscles and reveals changes in neural coupling [Pizzamiglio et al., 2017]. Reaching movements are among the most important recovery goals for post-stroke rehabilitation purposes, representing inter-joint coordination in activities of daily living [Moon et al., 2023]. Since reaching is one of the most common upper

limb movements used in daily life, it is also affected in cases of upper limb impairment, such as after a stroke. So, analysing reaching performance can be an indicator of functional recovery.

In this study, IMC was analysed and compared under 3 different conditions: 1) without using the exoskeleton (free conditions), 2) wearing the exoskeleton with a low level of assistance, and 3) wearing the exoskeleton with a high level of assistance. By observing the IMC variation across these three conditions, the effect of an external assistant provided by the exoskeleton was evaluated. The outcome of this study will enhance our knowledge and understanding of how wearable rehabilitation devices affect human motor control, enabling us to develop more effective rehabilitation tools for individuals with motor impairments.

Main Experimental Hypothesis (H1): There is an intermuscular coherence (IMC) modulation between agonist-antagonist muscle pairs when performing the reaching tasks under different conditions.

The main hypothesis suggests that external assistance provided by the exoskeleton, whether at low or high levels, affects motor coordination and consequently leads to modulation of IMC between the muscle pairs. The modulation may occur due to the exoskeleton's involvement in assisting the movement, potentially altering the normal interaction between agonist and antagonist muscles during the reaching tasks.

Null Hypothesis (H0): There is no IMC modulation between the

agonist-antagonist muscle pairs when performing the tasks under different conditions.

This hypothesis is based on the assumption that, in healthy subjects, the assistance provided by FLOAT (at both low and high levels) does not significantly interfere with motor coordination patterns. In other words, because healthy individuals are capable of generating movements independently, external assistance (at any level) should not disrupt or alter the natural neural control mechanisms that regulate muscle coordination. Therefore, the IMC between the pairs of agonist-antagonist is expected to remain consistent in all conditions (free, low assistance, and high assistance).

The data used in this study belongs to the NEBULA (Neuromechanical Biomarkers for Upper Limb Assessment) project, which is the doctoral research of my colleague, Florencia Garro. All the steps and procedures I will explain in the following sections were conducted within the NEBULA framework. [Garro et al., 2023]

2.2 Participants

Twenty healthy adult subjects (mean age: 31+/-6 years; 10 females, 10 males), all right-handed and with no recent upper limb surgery, volunteered to participate in the study. Participants were informed about the experi-

mental procedures and provided their consent to participate in the study. Individuals who met the following conditions were excluded from the study:

- Chronic inflammatory diseases affecting the right upper limb joints;
- Severe osteoporosis in the spine or right upper limb;
- Spinal fractures or instability;
- Orthopedic conditions limiting right upper extremity function;
- Significant contractures in the trunk or right upper limb;
- Skin integrity issues near device contact areas;
- Neuro-muscular disorders;
- Pregnancy or lactation.

The study and its procedures were approved by the local ethics committee (CER Liguria:784/2022 - DB id 12044)

2.3 Experimental setup

2.3.1 Float exoskeleton

The FLOAT exoskeleton is an assistive device for upper limb rehabilitation, developed at the Rehab Technologies lab at the Italian Institute of

Technology (IIT, Genoa). This advanced robotic device represents an innovative approach to addressing the challenges of robotic rehabilitation, designed specifically to promote and accelerate motor and functional recovery of the shoulder joint complex following post-traumatic or post-surgical injuries [Buccelli et al., 2022]. The system consists of five rotational joints, providing five degrees of freedom, which are sufficient for performing daily movements and activities.

The system's key innovation lies in its passive, polyarticulated arm, which supports the total exoskeleton weight while allowing patients to move freely within very large workspaces, enabling deeper interaction with the surrounding environment. This design philosophy recognizes that effective rehabilitation requires not only mechanical assistance but also the preservation of natural movement patterns and opportunities for environmental interaction. Patients wearing FLOAT can perform a wide variety of activities of daily living without bearing the device's weight, addressing the acceptance and usability challenges that have previously limited the clinical adoption of other systems.

FLOAT provides adjustable support to assist patients with vertical arm movement during rehabilitation, with the system designed based on the natural weight of the human arm to ensure movements and support feel natural. When patients want to lift their arm, the assist mode provides an extra push during vertical upward movement. As the arm lowers, the support mode provides gentle resistance to prevent sudden and quick drops. The FLOAT system's control algorithms are designed to provide assistance that adapts to user intention and movement characteristics, with the intensity of assistance

selectable among three levels: low, medium, and high. This allows for different levels of support based on the patient's comfort and the stage of recovery. This adaptability represents a significant advancement over earlier systems that provided fixed assistance patterns regardless of patient capability or movement context.

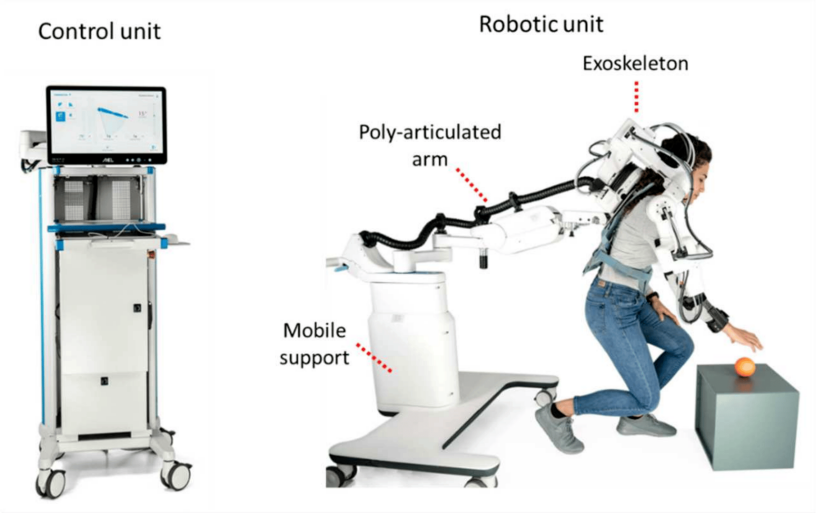

Figure 2.1: Float exoskeleton system. Two main units: a control unit that allows supervising the rehabilitation sessions, and a robotic unit that includes the exoskeleton itself with polyarticulated arm and mobile support for free movement in a large space and performing activities without feeling the weight of the device on the arm. [Buccelli et al., 2022]

2.3.2 Touch panel

To perform the standardized, self-paced reaching task for the study, an adaptable touch panel was designed as the central interface for participants while they were seated on an adjustable chair wearing the exoskeleton. The panel consists of 9 targets, each providing three levels of height and three levels of lateral placement, positioned with the participant's medial plane and shoulder complex. Each target was equipped with a light indicator switching on and off to indicate the randomized sequence of 10 repetitions for each of the 9 targets on the panel. [2.2]

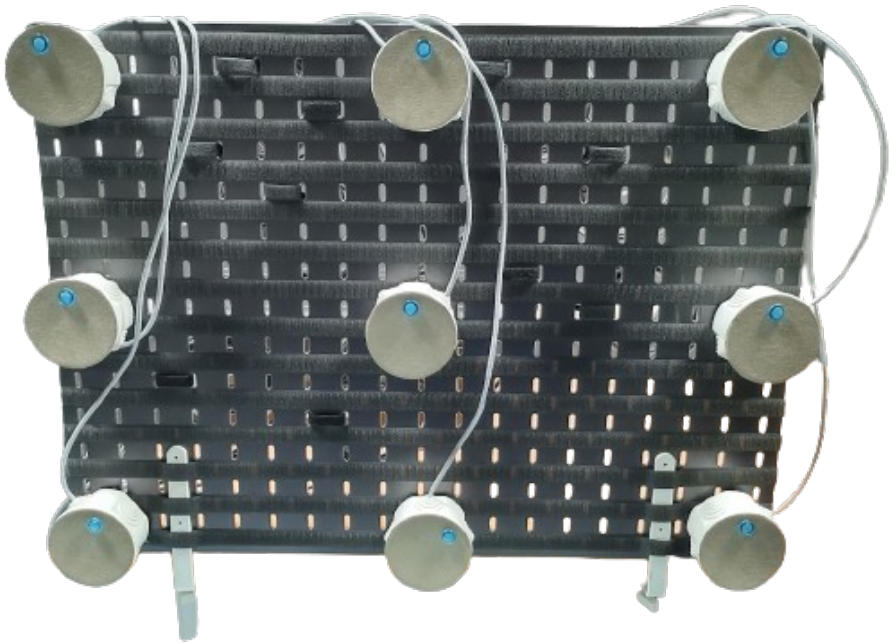

Figure 2.2: Adjustable Touch Panel

2.3.3 EMG system

EMG data was collected from the muscles of the right shoulder, upper arm, and forearm by wireless EMG sensors using the Cometa Waveplus system at a sampling frequency of 1000 Hz. The use of wireless sensors ensured participants' comfort and minimized setup time.

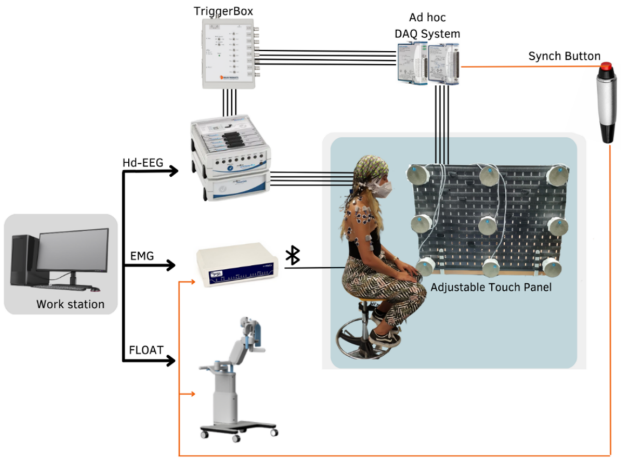

Figure 2.3: The setup of the study. The touch panel system is synchronized with a wireless surface EMG recorder, and the exoskeleton using a synchronization button corresponding to all the systems.[Garro et al., 2023]

2.3.4 Muscle Selection

To effectively assess intermuscular coherence (IMC), it is essential to consider the functional relationships between muscles, particularly agonist–antagonist pairs. Agonist muscles initiate and drive movement through contraction, while antagonist muscles provide opposing forces that help regulate and stabilize the motion. This balance between activation and inhibition ensures that joint actions remain smooth, controlled, and precisely coordinated. Computing coherence between these muscle pairs offers valuable insight into how the nervous system coordinates motor control, particularly under varying movement conditions, such as unassisted motion or when different levels of external support are provided. The specific muscle pairs considered as agonist and antagonist in this study are supported by established findings in the relevant literature [Wierzbicka et al., 1986] are listed below:

- **Biceps Brachii — Triceps Brachii:** These muscles form an agonist-antagonist pair. The biceps, located on the front of the upper arm, is primarily responsible for elbow flexion and also contribute to shoulder motion by helping in abduction, adduction, flexion, and forearm supination. The Triceps Brachii, located on the back of the upper arm, is responsible for elbow extension and also assists in shoulder extension and adduction.

- **Anterior Deltoid — Posterior Deltoid:** These muscles form an important agonist-antagonist pair, each playing a crucial role in shoulder movement. The Anterior Deltoid, located on the front of the

shoulder, facilitates shoulder flexion, medial rotation, and abduction. In contrast, the Posterior Deltoid, located at the back of the shoulder, supports shoulder extension, lateral rotation, and abduction.

- **Pectoralis Major — Posterior Deltoid:** These muscles act antagonistically in many upper-body movements, such as reaching. The Pectoralis Major, located on the front of the chest, is responsible for adduction and internal rotation, while the Posterior Deltoid, positioned at the back of the shoulder, contributes to shoulder extension and abduction.

- **Middle Trapezius — Pectoralis Major:** The Middle Trapezius, located in the upper back, retracts the scapula, contrasting with the Pectoralis Major, which aids in shoulder adduction, internal rotation, and, depending on its fixed point, can also elevate the chest during forced inhalation. Also, it is essential for maintaining proper posture and stabilizing the shoulder during various activities.

- **Upper Trapezius — Lower Trapezius:** This muscle pair stabilizes the scapula, with the Upper Trapezius located at the top of the back and neck, elevating and laterally rotating the scapula, and the Lower Trapezius positioned at the lower part of the upper back, aiding in its depression and upward rotation.

- **Extensor Carpi Ulnaris — Biceps:** The Extensor Carpi Ulnaris, located in the posterior compartment of the forearm, is primarily responsible for extending and adducting the wrist. While these muscles

act on different joints, they often work in coordination during activities that combine elbow flexion and wrist extension, like lifting and carrying objects. This coordination helps create smooth and efficient movement in the upper limb, enabling better control and strength during everyday actions.

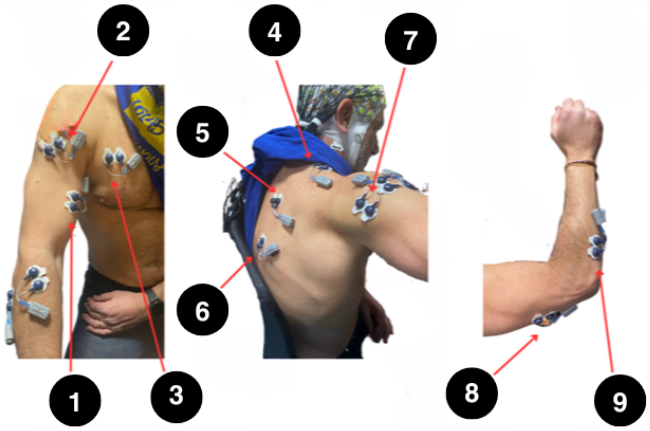

Figure 2.4: Muscles involved in the data collection: 1) Biceps Brachii, 2) Anterior Deltoid, 3) Pectoralis Major, 4) Upper Trapezius, 5) Medial Trapezius, 6) Lower Trapezius, 7) Posterior Deltoid, 8) Triceps Brachii, 9) Extensor Carpi Ulnaris.

2.3.5 Frequency Range

The frequency range considered in this study is the beta band, which, based on the literature, is between 13 and 30 Hz, and is considered the most suitable range for studies related to motor control and motor coordination. In this study, however, the frequency range was adjusted to 11.5 - 31.25 Hz to ensure precise analysis of the beta band (13-30 Hz). This adjustment was necessary due to the frequency bin resolution of the analysis method. By extending the lower limit to 11.5 Hz and the upper limit to 31.25 Hz, the frequency bins could be aligned to capture the complete 13 - 30 Hz beta band range. This modification ensured that the full spectrum of beta band motor-related activity was accurately captured, allowing for a more comprehensive understanding of IMC analysis during the reaching task. Additionally, exploratory analyses were conducted on the alpha (6-12 Hz) and gamma (30-60 Hz) frequency bands to investigate potential motor-related activity beyond the beta range. The procedures and results of these supplementary analyses are presented in Appendix.

2.4 Experimental protocol

2.4.1 Standardized Reaching Task

The task investigated in the study is reaching toward the targets of a touch panel. The time sequence was manually recorded by a push button to indicate

the start and end of reaching. Subjects were seated in front of an adjustable touch panel, whenever the integrated LED light on each target was switched on, subjects could start the movement toward the target, and at the same time a push button was pressed to record the start timing of movement and it was sent to the working station and thanks to its capacitive cover, it allows the recording of the movement duration. When the subject reaches the target, a push button is pressed to capture the movement's end time.

2.5 Data Analysis

The data analysis framework contains the following steps :

2.5.1 Preprocessing

Digital Filtering

The raw EMG signals were preprocessed to remove artifacts while preserving the oscillatory information essential for intermuscular coherence (IMC) analysis. This preprocessing stage is crucial due to the intrinsic noise present in EMG recordings obtained from surface electrodes, and it aims to enhance signal quality by eliminating noise and artifacts. A two-stage filtering approach was implemented for each of the EMG channels to ensure that the data retained only physiologically relevant components for subsequent analysis. First, a 2nd-order Butterworth notch filter with a stopband of 49-51 Hz was applied to eliminate 50 Hz powerline interference and its harmonics. This narrow stopband effectively removed powerline noise while minimizing distortion of the surrounding frequency components.

Subsequently, a 4th-order Butterworth high-pass filter with a cutoff frequency of 10 Hz was applied to remove low-frequency movement artifacts and baseline drift. The 10 Hz cutoff was specifically chosen to preserve the beta band oscillations, which are the primary frequency range of interest for corticomuscular coupling during voluntary movements. Both filters were applied using zero-phase digital filtering (filtfilt function) to prevent phase distortion that could compromise the subsequent coherence analysis.

Event-Based Segmentation

Following filtering, the continuous EMG recordings were segmented into task-relevant epochs based on experimental event markers. Event labels containing extraneous spaces were first cleaned to ensure consistent marker detection. The segmentation algorithm identified movement onset markers ("G" for Go) followed by reach completion markers ("R" for Reach), extracting the EMG activity between these temporal boundaries. This approach yielded discrete epochs for each reaching movement, resulting in up to 90 epochs per subject per condition (9 targets $\times$ 10 repetitions), with each epoch capturing the complete reaching phase from movement initiation to termination.

2.5.2 IMC computation

Following preprocessing and epoching, intermuscular coherence (IMC) was computed to quantify the frequency-specific synchronization between muscle pairs during reaching movements. For each epoch, the power spectral densities (PSDs) and cross-spectral density (CSD) were estimated using Welch's method with a 512-sample Hamming window (512 ms duration), 50% over-

lap (256 samples), and 512-point FFT, yielding a frequency resolution of approximately 1.95 Hz. This window length was selected to provide adequate frequency resolution for the beta band while maintaining sufficient temporal resolution across the movement duration. The magnitude-squared coherence was subsequently calculated as:

$$IMC_{(f)} = \frac{|CSD_{xy}(f)^2|}{[PSD_{xx}(f) \cdot PSD_{yy}(f)]} \tag{2.1}$$

Where IMC(f) represents the intermuscular coherence between EMG signal x and y at frequency f. PSDxx(f) and PSDyy(f) are the auto–power spectral densities of signals x and y, respectively, while CSDxy(f) denotes the cross–spectral density between x and y.

The resulting coherence values range from 0 to 1, where 0 indicates no linear relationship and 1 indicates perfect linear coupling at a given frequency.

The computed coherence spectra were stored in a six-dimensional matrix structure (subjects × conditions × targets × repetitions × muscle pairs × frequencies), facilitating subsequent statistical analysis across the experimental factors. IMC values were subsequently averaged across repetitions and subjects to yield a representative coherence spectrum for each target-condition-muscle pair combination, reducing measurement variability while preserving the spatial specificity of the reaching task.

2.5.3 Statistical Analysis

A comprehensive statistical framework was implemented to assess the effects of assistance conditions on IMC patterns. The statistical approach was designed to provide precise testing of hypotheses using within-subject comparisons across different assistance conditions.

Normality Test: Before selecting appropriate statistical tests, the Shapiro-Wilk test (swtest) was applied to assess the normality of coherence data distributions for each muscle pair and condition. The normality assessment was crucial for determining whether parametric or non-parametric statistical methods were appropriate for the subsequent analyses. The test was performed on the coherence values to determine whether the data met the assumptions required for parametric statistical tests. The Shapiro-Wilk test was chosen over other normality tests due to its high statistical power in detecting departures from normality, particularly in small to moderate sample sizes, which are typical of neurophysiological studies.

Results indicated that the majority of distributions deviated significantly from normality ($p < 0.05$), necessitating the use of non-parametric statistical methods. The violation of normality assumptions ruled out the use of parametric tests such as repeated-measures ANOVA and guided the selection of appropriate non-parametric alternatives.

Friedman Test: Given the non-normal distribution of the coherence data and the within-subject experimental design involving three conditions, the Friedman test was employed as the primary statistical analysis. The Friedman test is a non-parametric repeated-measures statistical procedure that

evaluates differences across multiple conditions, within the same group of subjects, without requiring assumptions of normality or homoscedasticity, making it appropriate for the characteristics of the present dataset.

The test was applied to coherence data that had been averaged over repetitions for each target for each subject, resulting in a single coherence value per subject per condition per target for each muscle pair.

This approach determined whether the overall distribution of coherence values differed significantly across the three experimental conditions. Each reaching target was treated as a distinct task condition and analyzed separately, as the targets differed in spatial location and therefore required different movement trajectories and postural configurations. Reaching movements toward upward versus lateral targets are known to engage different coordination strategies, and intermuscular coherence has been shown to depend on task characteristics and limb posture. For this reason, Friedman tests were performed separately for each target to explore target-specific modulation of IMC across assistance conditions.

At the same time, we acknowledge that targets cannot be considered fully independent observations, as all movements were performed by the same subjects within the same experimental session. Consequently, factors such as individual motor control strategies, adaptation to the task, and fatigue are shared across targets and may introduce correlations between measurements. While the adopted approach enables investigation of spatial sensitivity of IMC modulation across the workspace, it may overestimate the apparent robustness of condition-related effects when statistical significance is evaluated separately across targets. Future studies could address this limitation

by aggregating coherence measures across targets or by applying statistical models that explicitly account for within-subject and within-target dependencies, such as mixed-effects models.

The Friedman test is robust to outliers and non-normal distributions, making it particularly suitable for coherence data. A significant Friedman test ($p < 0.05$) indicated that at least one condition differed significantly from the others, warranting further post-hoc analysis to identify specific pairwise differences.

Wilcoxon signed-rank test: The Wilcoxon signed-rank test assesses whether the median difference between paired observations is statistically significant, offering a suitable non-parametric approach for post-hoc comparisons.

Three specific pairwise comparisons were conducted:

- Free vs. Low assistance
- Free vs. High assistance
- Low assistance vs. High assistance

False Discovery Rate (FDR) Correction: To account for multiple comparisons while maintaining adequate statistical power, the False Discovery Rate (FDR) correction procedure developed by Benjamini and Hochberg (1995) was applied using the positive dependency correction method ('pdep'). FDR correction controls the expected proportion of false positives among significant findings, rather than attempting to eliminate all false positives across

the entire set of tests. This approach is particularly appropriate for exploratory analyses with multiple tests, as it balances the need to control Type I errors while preserving sufficient power to detect genuine effects. The Benjamini-Hochberg procedure with positive dependency correction ('pdep') is particularly suitable for neurophysiological data where test statistics may exhibit positive correlation due to shared neural drive across targets.

The correction was applied hierarchically at two levels:

1. **Friedman test correction:** For each muscle pair, FDR correction was applied across the nine targets (9 tests per muscle pair), with the corrected significance threshold set at $\alpha = 0.05$. This controlled the false discovery rate within each muscle pair's set of target-specific comparisons.

2. **Post-hoc pairwise comparison correction:** For each muscle pair, FDR correction was applied across all pairwise comparisons (9 targets $\times$ 3 pairwise comparisons = 27 tests per muscle pair), again using $\alpha = 0.05$. This controlled the false discovery rate across the entire set of post hoc tests for each muscle pair.

The FDR procedure was implemented separately for each muscle pair rather than globally across all muscle pairs to maintain interpretability and recognize the a priori theoretical interest in each muscle pair's response pattern.

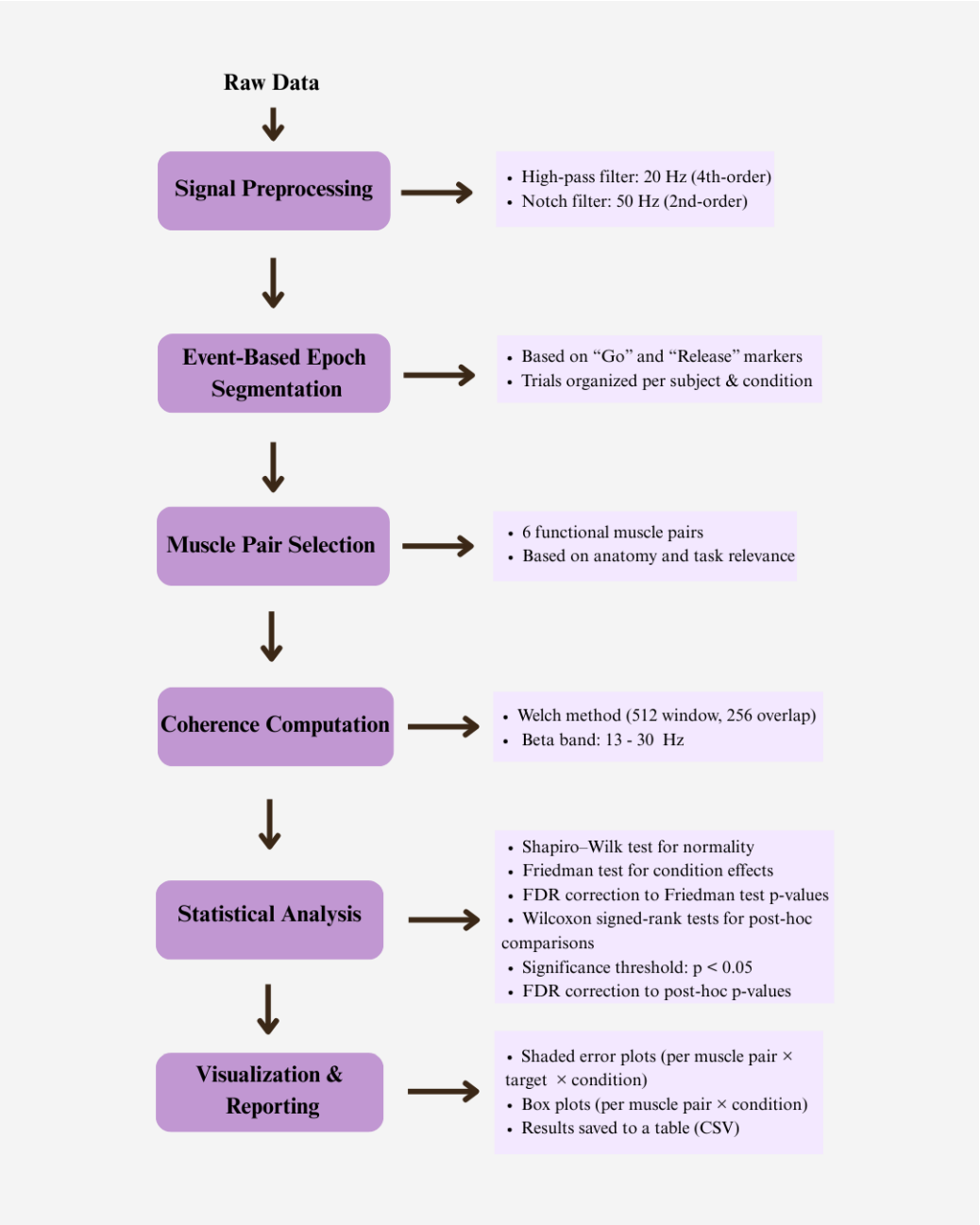

Figure 2.5: Schematic representation of the EMG signal processing and intermuscular coherence analysis pipeline.

Chapter 3

Results

3.1 Results of IMC analysis

The present study was designed to investigate whether intermuscular coherence (IMC) patterns during reaching movements in healthy participants are modulated by robotic assistance. Based on the evidence suggesting the role of IMC as a biomarker of neural coordination, it was hypothesized that natural coordination patterns between agonist-antagonist muscle pairs would be altered by external mechanical assistance (H1: IMC modulation between agonist-antagonist muscle pairs occurs when reaching tasks are performed under different assistance conditions). This hypothesis was grounded in the expectation that neural drive and coordination strategies required for movement execution would be influenced by robotic assistance, even in healthy individuals. Conversely, the null hypothesis (H0) proposed that IMC patterns would not be significantly affected by robotic assistance, suggesting that healthy individuals' robust motor control systems would maintain con-

sistent neural coordination regardless of external assistance levels.

To test these hypotheses, beta-band coherence (13-30 Hz) patterns were examined across six functionally relevant muscle pairs representing key functional relationships across the upper extremity: Biceps-Triceps (elbow flexion/extension), Anterior Deltoid-Posterior Deltoid (shoulder flexion/extension), Pectoralis Major-Posterior Deltoid (shoulder adduction/extension), Middle Trapezius-Pectoralis Major (shoulder stabilization/adduction), Upper Trapezius-Lower Trapezius (shoulder elevation/depression), and Biceps-Extensor Carpi Ulnaris (elbow flexion/wrist extension). Participants performed 10 repetitions of reaching movements to nine targets in a randomized order under three experimental conditions: free movement without assistance, low-level robotic assistance, and high-level robotic assistance. IMC was computed using cross-spectral density and power spectral density estimates for each muscle pair, employing MATLAB's pwelch and cpsd functions. The findings provide strong support for the experimental hypothesis (H1), demonstrating significant modulation of IMC across all examined muscle pairs when robotic assistance was provided, thereby rejecting the null hypothesis (H0).

Visual inspection of the coherence spectra across all nine reaching targets revealed consistent patterns of IMC modulation in response to robotic assistance. The beta-band coherence (13-30 Hz) plots for each of the six muscle pairs showed clear condition-dependent differences across all experimental conditions and reaching targets (Figures 3.1-3.6). Across all muscle pairs and targets, a consistent pattern of coherence reduction was observed when robotic assistance was provided, with free movement conditions demon-

strating higher coherence values compared to both low-assistance and high-assistance conditions.

Before performing the main statistical analysis, data normality was assessed using the Shapiro-Wilk test for each pair of muscles and combination of conditions. Results indicated that the majority of datasets violated normality assumptions ($p < 0.05$), necessitating the use of non-parametric statistical methods. Consequently, the Friedman test was employed as the overall test to evaluate differences between the three conditions for each muscle pair. Following the Friedman test, post-hoc pairwise comparisons were conducted using the Wilcoxon signed-rank test to identify specific differences between conditions, with FDR correction applied as described in the previous chapter.

The analysis revealed that robotic assistance consistently altered intermuscular coherence patterns across the majority of examined muscle pairs (Figures 3.1-3.6). All six muscle pairs demonstrated significant overall effects in the Friedman test , indicating that the assistance conditions produced systematically different coherence values. Post-hoc analysis revealed significant differences in the majority of pairwise comparisons, with a clear pattern emerging: all significant differences were observed between free movement and assisted conditions (either low or high assistance), while no significant differences were found between the two assistance levels themselves.

The following sections provide detailed analyses of IMC modulation for each muscle pair, including boxplot visualizations and statistical findings comparing coherence distributions across assistance conditions.

3.1.1 Biceps Brachii — Triceps Brachii

Analysis of intermuscular coherence between the biceps and triceps revealed a significant modulation by robotic assistance in the beta frequency band. Box plot analysis (Figure 3.1) confirmed these visual observations, revealing substantial differences between conditions with median coherence values of approximately 0.37 for free movement and 0.29 for low and high assistance conditions. The distribution of individual subject data points demonstrated consistent within-subject patterns. Notable inter-individual variability was observed, with coherence values ranging from 0.15 to 1 in the free condition, yet the pattern of assistance-induced reduction remained consistent across participants.

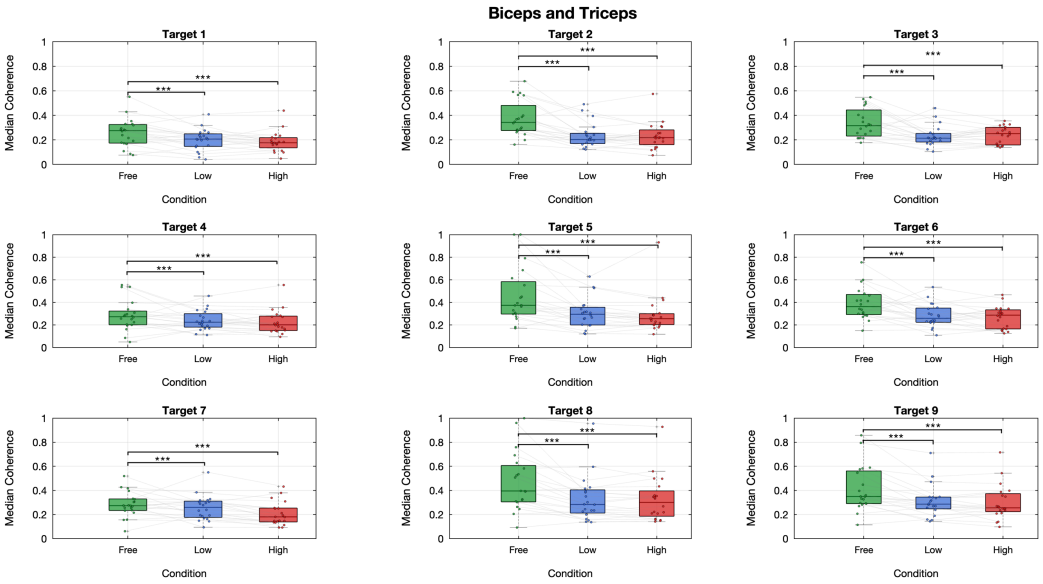

Figure 3.1: Biceps and Triceps beta-band coherence boxplot. Individual data points are overlaid on each box.

Statistical analysis supported these findings, with significant Friedman tests ($p < 0.05$) observed for the majority of targets across muscle pairs, indicating overall differences between assistance conditions. Post-hoc Wilcoxon signed-rank tests with FDR correction revealed significant pairwise differences between Free movement and both assistance conditions. Specifically, Free vs. Low assistance showed significant differences in 7 out of 9 targets ($p < 0.05$ for all except Target 4 and 7), and Free vs. High assistance demonstrated significant differences in 8 out of 9 targets ($p < 0.05$ for all except Target 4). However, the comparison between Low and High assistance levels showed significant differences only in 1 target (Target 7: $p =$

0.0022), indicating that the coherence alteration occurs when transitioning from Free to assisted movement, with minimal additional change between the two assistance levels.

The strongest coherence reductions differed slightly between targets. For Free vs. Low assistance, the largest reductions were observed in Target 2 (reduction of 0.134, from 0.338 to 0.204, $p = 0.0005$), Target 8 (reduction of 0.127, from 0.399 to 0.272, $p = 0.0003$), and Target 6 (reduction of 0.125, from 0.379 to 0.254, $p = 0.0051$). For Free vs. High assistance, the largest reductions occurred in Target 5 (reduction of 0.129, from 0.381 to 0.252, $p = 0.0004$), Target 2 (reduction of 0.108, from 0.338 to 0.230, $p = 0.0006$), and Target 8 (reduction of 0.106, from 0.399 to 0.293, $p = 0.0002$). Notably, Targets 2 and 8 consistently demonstrated substantial coherence reductions across both assistance levels, while the specific ranking of other targets varied. This pattern demonstrates a clear Free > Assisted reduction across the majority of targets, but does not support a progressive response (Free > Low > High), as coherence values show minimal additional change between the Low and High assistance conditions.

3.1.2 Anterior Deltoid — Posterior Deltoid

The anterior deltoid and posterior deltoid muscles are essential for controlling shoulder movements, especially during flexion and extension involved in upper-limb reaching tasks.

The analysis of intermuscular coherence between the anterior and posterior deltoid revealed a pattern similar to the biceps-triceps muscle pair, demonstrating consistent reductions in coherence with robotic assistance.

Visual inspection of the boxplots shows that IMC is highest in the Free condition and reduced under assisted conditions. However, the anterior-posterior deltoid pair displays generally higher absolute coherence values (ranging approximately 0.4 - 0.7 across targets) compared to biceps-triceps (ranging approximately 0.2 - 0.6), suggesting stronger baseline synchronization in this shoulder muscle pair. Additionally, the anterior-posterior deltoid shows more compressed boxplot distributions with smaller interquartile ranges in several targets, indicating potentially more consistent inter-subject responses to robotic assistance at the shoulder joint level compared to the elbow joint.

The boxplot analysis (Figure 3.2) revealed median coherence values across the nine targets ranging from approximately 0.41 to 0.69 for Free movement, 0.37 to 0.52 for Low assistance, and 0.39 to 0.54 for High assistance conditions. The individual subject data points demonstrated moderate inter-individual variability, with coherence values spanning a broad range across all conditions and targets.

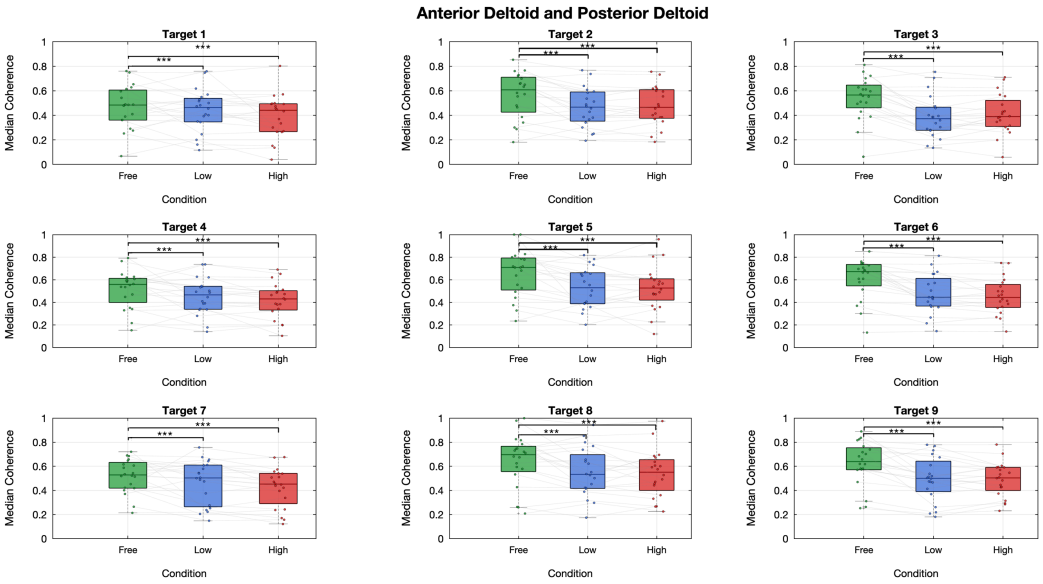

Figure 3.2: Anterior Deltoid and Posterior Deltoid beta-band coherence boxplot. Individual data points are overlaid on each box.

Statistical analysis supported these findings, with significant Friedman tests ($p < 0.05$) observed for the majority of targets across this muscle pair, indicating overall differences between assistance conditions. Post-hoc Wilcoxon signed-rank tests with FDR correction revealed significant pairwise differences between Free movement and both assisted conditions. Free vs. Low assistance showed substantial differences in 6 of 9 targets (all except Target 1, 4, and 7 ; $p < 0.05$), while Free vs. High assistance showed significant differences in all targets except target 1($p < 0.05$). However, Low vs. High assistance showed substantial differences in only 1 target (Target 7, $p = 0.0410$), indicating that the main decrease in coherence arises when moving from the Free to the assisted condition, with only minor further reduction

between the two assistance levels.

The largest coherence decreases varied across targets and comparisons. For Free vs. Low assistance, the largest reductions were observed in Target 6 (reduction of 0.228, from 0.673 to 0.445, p = 0.002), Target 3 (reduction of 0.193, from 0.566 to 0.373, p = 0.0031), and Target 5 (reduction of 0.179, from 0.709 to 0.530, p = 0.0085). For Free vs. High assistance, the largest reductions occurred in Target 6 (reduction of 0.23, from 0.673 to 0.443, p = 0.002), Target 5 (reduction of 0.182, from 0.709 to 0.527, p = 0.0051), and Target 3 (reduction of 0.176, from 0.566 to 0.390, p = 0.002). Notably, targets 6, 3, and 5 consistently demonstrated the most substantial coherence reductions across both assistance levels, appearing in the top three for both Free vs. Low and Free vs. High comparisons. This pattern demonstrates a clear Free > Assisted reduction across all targets, but does not support a progressive graded response (Free > Low > High), with minimal coherence reduction from Low to High assistance.

3.1.3 Pectoralis Major — Posterior Deltoid

The pectoralis major and the posterior deltoid form a critical antagonistic coupling that governs the horizontal shoulder dynamics during upper-limb movements. This muscular partnership is fundamental for controlling arm trajectory across the horizontal plane and ensuring precise endpoint positioning during reaching tasks.

Analysis of intermuscular coherence between the pectoralis major and posterior deltoid demonstrated consistent effects of robotic assistance. The boxplot analysis (Figure 3.3) revealed median coherence values across the

nine targets ranging from approximately 0.29 to 0.52 for Free movement, 0.19 to 0.33 for Low assistance, and 0.20 to 0.32 for High assistance conditions. The distribution patterns showed clear separation between the Free movement condition and both assisted conditions across most targets, while Low and High assistance conditions displayed considerable overlap with similar median values. Individual subject data points demonstrated generally consistent patterns, with the majority of participants showing the expected assistance-induced coherence reduction.

Statistical analysis supported these findings, with significant Friedman tests ($p < 0.05$) observed for all nine targets across this muscle pair, indicating overall differences between assistance conditions. Post-hoc Wilcoxon signed-rank tests with FDR correction revealed significant pairwise differences between Free movement and both assistance conditions across all 9 targets ($p < 0.05$ for Free vs. Low and Free vs. High assistance). However, Low vs. High assistance showed no significant differences in any of the nine targets, indicating that the primary coherence reduction occurs when transitioning from Free to assisted movement, with no additional measurable change between the two assistance levels.

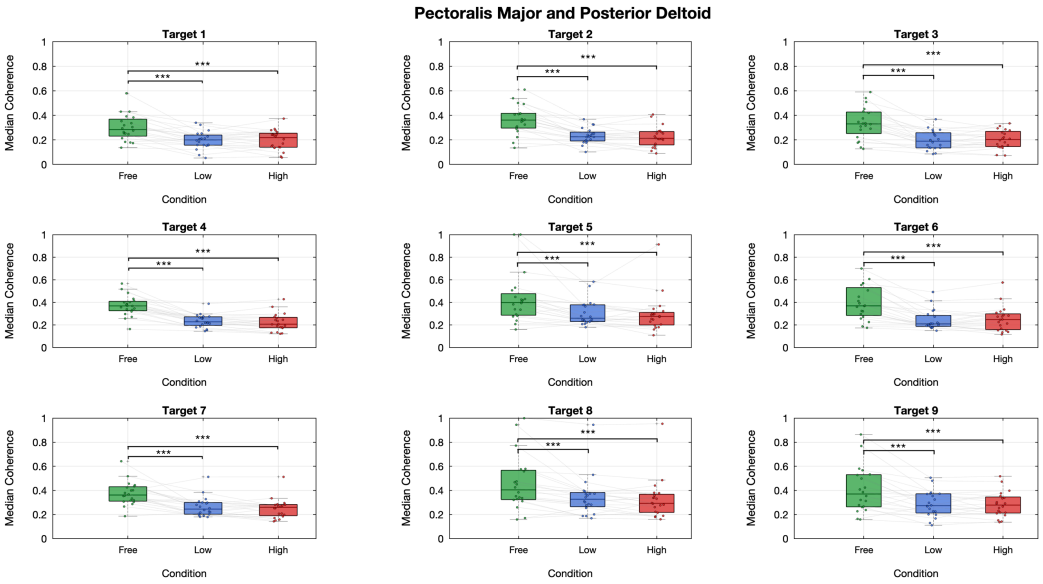

Figure 3.3: Pectoralis Major — Posterior Deltoid beta-band coherence boxplot. Individual data points are overlaid on each box.

The largest coherence reductions differed between the assistance levels. For Free vs. Low assistance, the largest reductions were observed in Target 6 (reduction of 0.16, from 0.369 to 0.209, $p = 0.0005$), Target 3,4,5 (reduction of 0.141), and Target 2 (reduction of 0.136, from 0.362 to 0.226, $p = 0.0005$). For Free vs. High assistance, the largest reductions occurred in Target 4 (reduction of 0.162, from 0.369 to 0.207, $p = 0.0005$), Target 2 (reduction of 0.149, from 0.362 to 0.213, $p = 0.0005$), and Target 3 (reduction of 0.128, from 0.331 to 0.203, $p = 0.0007$). Notably, Targets 2, 3, and 4 consistently demonstrated the most substantial coherence reductions across both assistance levels, appearing in the top three for both comparisons. This pattern demonstrates a clear Free > Assisted reduction across all targets, with Low and High assistance levels producing similar coherence magnitudes.

3.1.4 Middle Trapezius — Pectoralis Major

The middle trapezius and posterior deltoid constitute a stabilization-mobility coupling essential for scapular control and shoulder girdle positioning during reaching movements. This muscle pair controls two essential aspects of shoulder function: the middle trapezius maintains the shoulder blade's stability, while the pectoralis major enables the arm to move across the chest. Effective reaching requires coordination between these stabilizing and moving functions.

Analysis of intermuscular coherence between the middle trapezius and pectoralis major revealed substantial effects of robotic assistance. The boxplot analysis (Figure 3.4) showed median coherence values across the nine targets ranging from approximately 0.26 to 0.58 for Free movement, 0.18 to 0.32 for Low assistance, and 0.19 to 0.29 for High assistance conditions. The distribution patterns demonstrated separation between Free movement and both assisted conditions across all targets, while Low and High assistance conditions exhibited considerable overlap. Individual subject trajectories showed generally consistent downward trends from Free to assisted conditions across most targets.

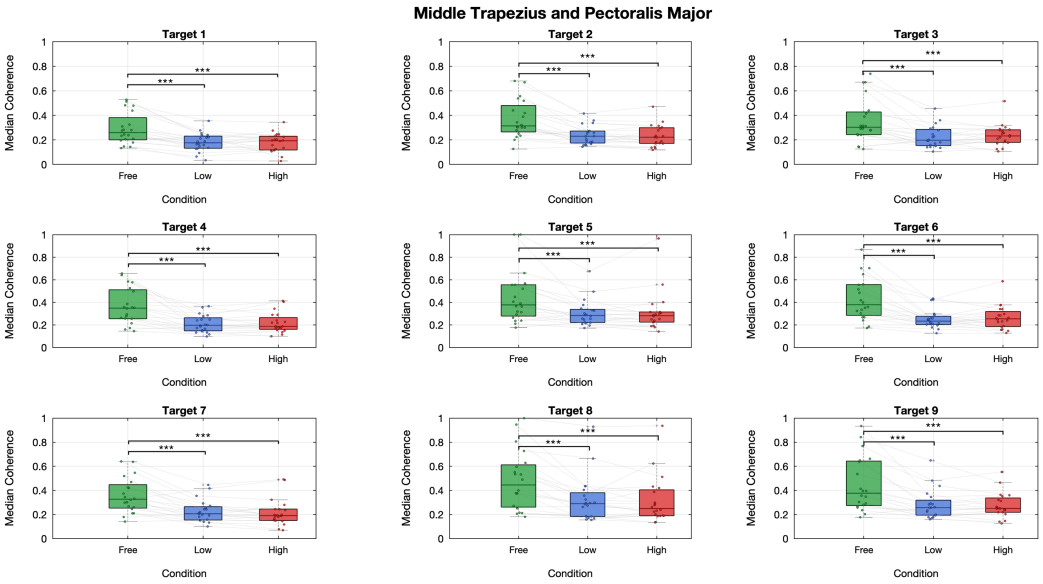

Figure 3.4: Middle Trapezius — Pectoralis Major beta-band coherence boxplot. Individual data points are overlaid on each box.

Statistical analysis supported these findings, with significant Friedman tests ($p < 0.05$) observed for all nine targets across this muscle pair, suggesting differences between assistance conditions. Post-hoc Wilcoxon signed-rank tests with FDR correction revealed significant pairwise differences between Free movement and both assistance conditions. Both Free vs. Low assistance and Free vs. High assistance showed significant differences in all 9 targets ($p < 0.05$). However, Low vs. High assistance showed no significant differences in any of the targets, suggesting that the main coherence decrease happens upon introducing robotic assistance, with negligible further changes between the two assistance magnitudes.

The largest coherence reductions were observed across multiple targets

and assistance levels, with Targets 8 and 4 appearing in the top two for both comparisons. For Free vs. Low assistance, the largest reductions were observed in Target 8 (reduction of 0.155, from 0.445 to 0.290, p = 0.0005), Target 4 (reduction of 0.152, from 0.348 to 0.196, p = 0.0005), and Target 6 (reduction of 0.145, from 0.379 to 0.234, p = 0.0005). For Free vs. High assistance, the largest reductions occurred in Target 8 (reduction of 0.196, from 0.445 to 0.249, p = 0.0008), Target 4 (reduction of 0.161, from 0.348 to 0.187, p = 0.0006), and Target 7 (reduction of 0.137, from 0.327 to 0.190, p = 0.0012). Targets 8 and 4 consistently exhibited the most substantial coherence reductions across both assistance conditions, while the third-ranked target varied (Target 6 for Low assistance, Target 7 for High assistance). This pattern demonstrates a clear Free > Assisted reduction across all targets, with both assistance levels producing comparable coherence values.

3.1.5 Upper Trapezius — Lower Trapezius

The pair of upper and lower trapezius muscles controls the movement and stability of the shoulder blade during reaching, requiring precise coordination between the increasing and depressing forces. Together, these muscles regulate scapular positioning and facilitate smooth shoulder mechanics during diverse upper limb tasks.

Intermuscular coherence analysis between the upper and lower trapezius demonstrated systematic changes induced by robotic assistance. Boxplot visualization (Figure 3.5) revealed median coherence values spanning approximately 0.24 to 0.40 during Free movement, 0.18 to 0.29 under Low assistance, and 0.19 to 0.28 with High assistance across the nine targets. Distribution

patterns showed distinct separation between Free and both assisted conditions for all targets, whereas Low and High assistance conditions displayed considerable overlap. Individual subject data exhibited predominantly clear decreases when transitioning from Free to assisted conditions.

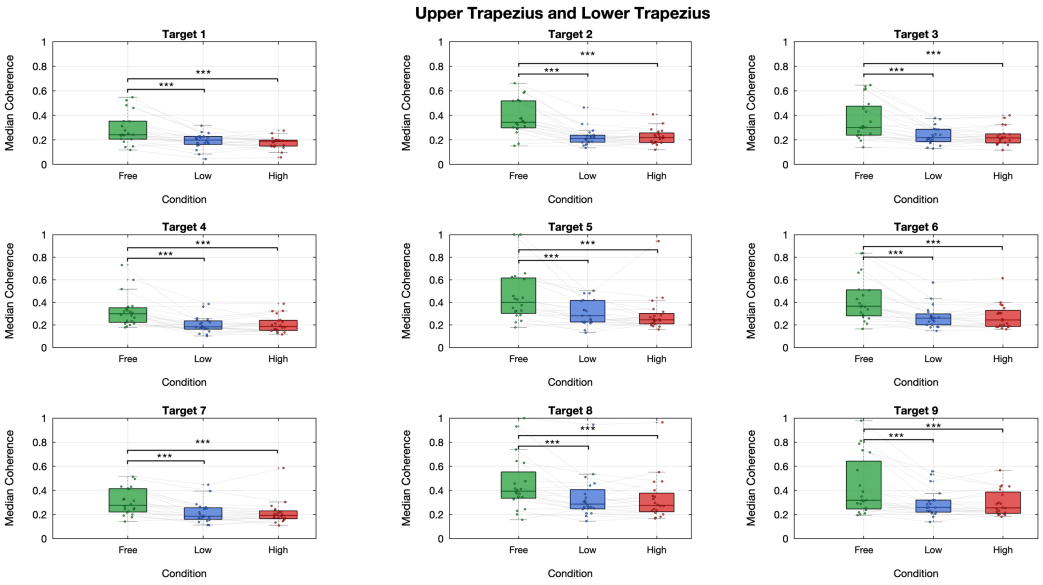

Figure 3.5: Upper Trapezius — Lower Trapezius beta-band coherence boxplot. Individual data points are overlaid on each box.

Statistical analysis supported these findings, with significant Friedman tests ($p < 0.05$) observed for all nine targets across this muscle pair, suggesting observable differences between assistance conditions. Post-hoc Wilcoxon signed-rank tests with FDR correction revealed significant pairwise differences between Free movement and both assistance conditions. Both Free vs. Low and Free vs. High assistance showed significant differences in all 9

targets ($p < 0.05$). However, comparisons between the two assistance levels revealed no significant differences for any target, showing that coherence changes are driven by whether assistance is present rather than how much assistance is provided.

The greatest coherence changes for Free vs. Low assistance were observed in Target 2 (reduction of 0.132, from 0.344 to 0.212, $p = 0.0005$), Target 5 (reduction of 0.118, from 0.400 to 0.282, $p = 0.0005$), and Target 4 (reduction of 0.116, from 0.299 to 0.183, $p = 0.0005$). For Free vs. High assistance, the largest reductions occurred in Target 5 (reduction of 0.155, from 0.400 to 0.245, $p = 0.0005$), Target 2 (reduction of 0.125, from 0.344 to 0.219, $p = 0.0005$), and Target 6 (reduction of 0.122, from 0.366 to 0.244, $p = 0.0005$). Target 2 and Target 5 consistently demonstrated the most substantial coherence reductions across both assistance conditions, alternating between first and second positions, while the third-ranked target differed between comparisons. This pattern demonstrates a clear Free > Assisted reduction across all targets, indicating that the introduction of assistance, rather than its magnitude, is the primary factor driving coherence alteration.

3.1.6 Extensor Carpi Ulnaris — Biceps

The biceps brachii and extensor carpi ulnaris represent a multi-joint coordination pattern that links elbow flexion with wrist stabilization during reaching movements. This pairing examines how the nervous system coordinates proximal arm control (elbow flexion) with distal forearm stabilization (wrist extension) to ensure proper hand positioning and grip preparation during target-directed reaching tasks.

Boxplot visualization (Figure 3.6) revealed median coherence values across the nine targets ranging from approximately 0.25 to 0.40 for Free movement, 0.18 to 0.29 for Low assistance, and 0.17 to 0.29 for High assistance conditions. Distribution patterns showed clear delineation between Free and both assisted conditions for most targets, with Low and High assistance levels displaying substantial overlap. Individual subject data demonstrated variable coherence values during Free movement, yet most participants exhibited consistent reductions when robotic assistance was introduced.

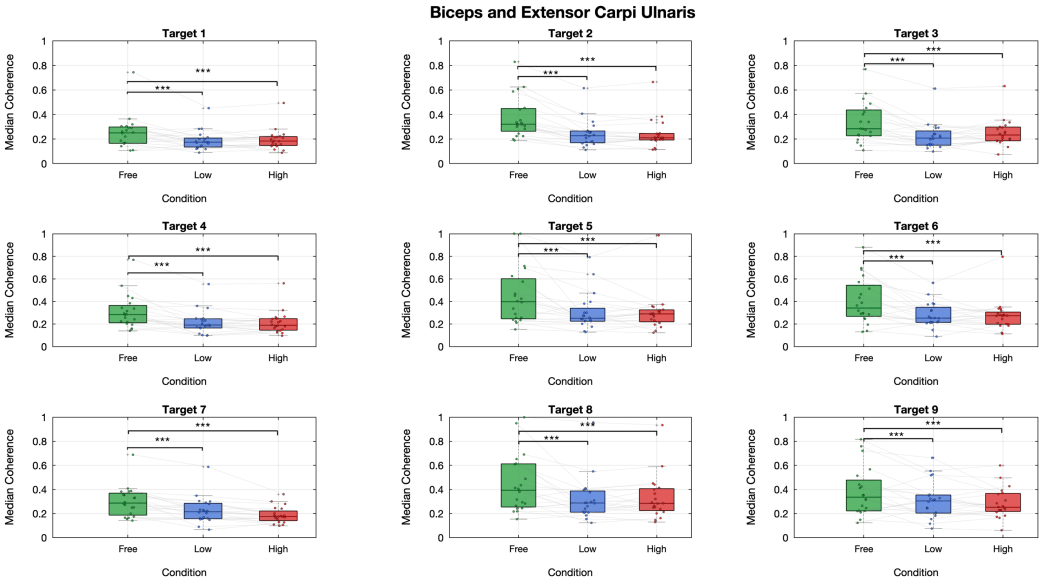

Figure 3.6: Extensor Carpi Ulnaris – Biceps beta-band coherence boxplot. Individual data points are overlaid on each box.

Statistical analysis corroborated these findings, with significant Friedman tests ($p < 0.05$) observed for 8 out of 9 targets across this muscle pair (all

except Target 9), indicating overall differences between assistance conditions for the majority of targets. Post-hoc Wilcoxon signed-rank tests with FDR correction revealed significant pairwise differences between Free movement and both low and high assistance conditions. Free vs. Low assistance showed significant differences in 8 of 9 targets (all except Target 9; $p < 0.05$), and Free vs. High assistance showed significant differences in all targets ($p < 0.05$). However, Low vs. High assistance showed significant differences only in 1 target (Target 7, $p = 0.0414$), suggesting that coherence changes are driven by whether assistance is present rather than how much assistance is provided.

The most substantial coherence reductions varied between assistance levels. For Free vs. Low assistance, the largest reductions were observed in Target 5 (reduction of 0.147, from 0.398 to 0.251, $p = 0.0051$), Target 8 (reduction of 0.105, from 0.392 to 0.287, $p = 0.0106$), and Target 2 (reduction of 0.094, from 0.321 to 0.227, $p = 0.0009$). For Free vs. High assistance, the largest reductions occurred in Target 7 (reduction of 0.112, from 0.287 to 0.175, $p = 0.0009$), Target 2 (reduction of 0.111, from 0.321 to 0.210, $p = 0.0009$), and Target 5 (reduction of 0.109, from 0.398 to 0.289, $p = 0.0173$). Targets 2 and 5 consistently appeared among the most affected targets across both assistance conditions, though their relative ranking varied. This pattern demonstrates a clear Free > Assisted reduction across the majority of targets, with the two assistance levels producing comparable effects.

While the reduction from free movement to assisted conditions reached statistical significance, the magnitude of these changes was relatively small compared to other muscle pairs examined. These findings may suggest several

possibilities for proximal-distal coordination under external support, though definitive conclusions remain elusive.

3.1.7 Target-Specific Sensitivity to Robotic Assistance

Beyond muscle-pair differences, analysis of target-specific coherence changes revealed that some reaching directions showed greater consistency in sensitivity to robotic assistance across multiple muscle pairs. Target 2 showed the greatest sensitivity, ranking among the top three targets with the largest coherence reductions across six muscle pairs in both assistance conditions. Targets 5 (center position) and 6 similarly demonstrated high sensitivity, each appearing in the top three for five muscle pairs. Target 8 and Target 3 (left-center direction) showed moderate consistency, appearing in four muscle pairs each. In contrast, Targets 1, 7, and 9 demonstrated less consistent sensitivity across muscle pairs.

This spatial pattern suggests that robotic assistance effects are not uniformly distributed across the reaching workspace. Forward and lateral reaching directions (particularly Targets 2, 5, and 6) appear to elicit more pronounced coordination changes across multiple muscle pairs compared to backward or extreme lateral targets.

To visualize the spatial distribution of assistance-induced coherence changes across the reaching workspace, targets are color-coded in Figure 3.7 based on their sensitivity to robotic assistance. Target sensitivity was determined by counting how frequently each target appeared among the top three targets with the largest coherence reductions across all six muscle pairs

and both assistance conditions (Free vs. Low and Free vs. High). Targets are displayed with varying shades of red, where darker red indicates higher consistency in showing large coherence changes across multiple muscle pairs (Target 2: darkest, appearing in 6 muscle pairs; Targets 5 and 6: medium-dark, appearing in 5 muscle pairs each), and lighter shades represent targets with less consistent sensitivity. This may reflect biomechanical differences in how the robotic exoskeleton supports movements toward different workspace locations, or differential reliance on specific muscle coordination strategies depending on target position and movement direction.

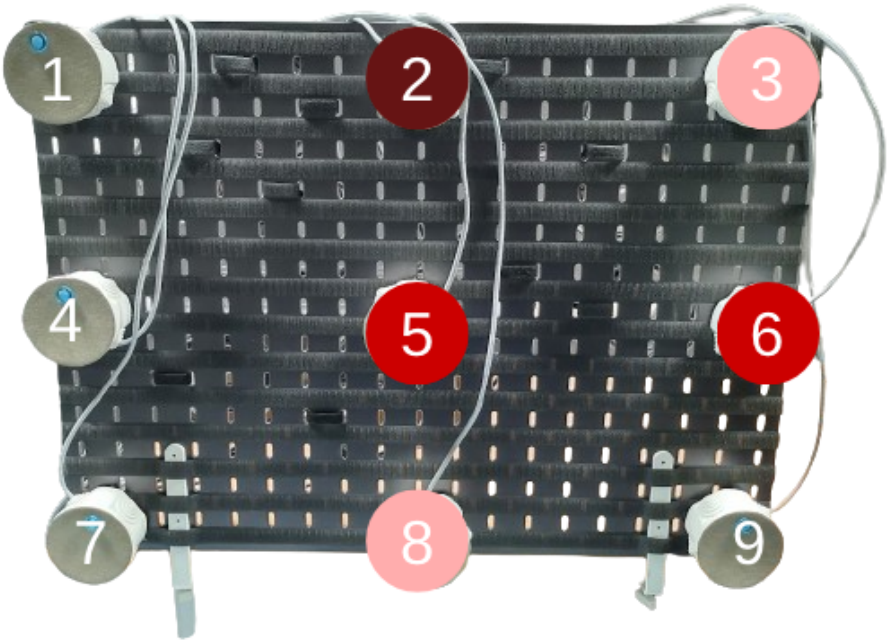

Figure 3.7: Spatial distribution of target sensitivity to robotic assistance.

Chapter 4

Discussion

4.1 Principal findings and neurophysiological interpretations

The present study investigated the effects of robotic assistance on intermuscular coordination patterns during reaching movements in healthy individuals. Through a comprehensive analysis of beta-band (13-30 Hz) intermuscular coherence across six agonist-antagonist muscle pairs, consistent and significant alterations in neuromuscular coordination strategies were identified when external support was provided. These findings may provide novel insights into how the central nervous system alters motor control strategies in response to mechanical assistance, with important implications for understanding human-robot interaction during upper limb movements.

4.1.1 Consistent response pattern across muscle pairs

The main finding of this investigation was the consistent reduction of IMC between free and assisted modalities across all pairs of muscles, supporting the hypotheses of this work. Friedman tests revealed significant overall differences between conditions for all examined muscle pairs (all $p < 0.05$ after FDR correction), indicating potentially meaningful changes. Post-hoc pairwise comparisons using Wilcoxon signed-rank tests with FDR correction demonstrated that all muscle pairs showed statistically significant reductions in beta-band coherence when comparing free movement to both assisted conditions ($p < 0.05$ after correction). This consistent response pattern suggests that robotic assistance induces fundamental changes in intermuscular coordination that transcend specific anatomical or functional muscle relationships.

Although the magnitude of these coherence reductions varied between muscle pairs, the direction of change remained remarkably consistent across all examined pairs. This systematic pattern indicates a fundamental reorganization of neuromuscular control strategies in response to mechanical assistance, rather than random or muscle-specific adaptations.

4.1.2 Individual variability in response to robotic assistance

A key observation from this study was the considerable inter-subject variability in how participants responded to robotic assistance. Individual IMC values in the unassisted condition span a wide range across participants, and the trajectories of change across assisted conditions are not uniform.

While some participants showed clear modulation of their intermuscular coherence in response to robotic assistance "responders", others exhibited minimal changes regardless of the assistance condition "non-responders". **A**t the group level, no significant differences in coherence values were found between low and high assistance conditions for any muscle pair ($p > 0.05$ for all comparisons), although both assisted conditions differed significantly from unassisted movement. No statistically significant differences were detected between low and high assistance levels. This finding may reflect the substantial individual heterogeneity observed in the data (Figures 3.1-3.6), where individual participants showed varied and often opposing responses to the two magnitudes of assistance, as evidenced by the divergent trajectories between conditions. When analyzing the overall distribution across all participants using rank-based statistics, opposing patterns of change in different individuals (some showing increases, others showing decreases) could cancel out, masking subject-specific sensitivities to the magnitude of assistance. For some participants, even a low level of assistance may be sufficient to elicit a maximal shift in coordination strategy, resulting in a plateau effect where additional assistance does not produce further change. For others, the assistance levels provided may not have been sufficient to trigger measurable alterations in intermuscular coordination, potentially due to differences in baseline motor control strategies or task adaptation.

A more detailed exploration of intra-subject variability, including characterization of responder and non-responder profiles, represents an important direction for future research but is beyond the scope of the present work.

4.1.3 Differential Sensitivity Across Muscle Pairs

While all muscle pairs demonstrated consistent significant coherence reductions, considerable variation in the magnitude and frequency of these effects was observed across different muscle combinations. The strongest and most consistent effects were demonstrated by three muscle pairs showing significant differences across all nine reaching targets: pectoralis major-posterior deltoid, middle trapezius-pectoralis major, and biceps-triceps. These pairs exhibited not only universal significant changes across all targets but also the largest magnitudes of coherence reduction, suggesting that scapular-pectoral coordination, shoulder adduction-extension control, and elbow flexion-extension are particularly sensitive to external mechanical support.

The upper trapezius-lower trapezius pair and biceps-extensor carpi ulnaris pair also showed significant changes across all nine targets, though with relatively smaller effect magnitudes. This reveals that scapular elevation-depression coordination and multi-joint elbow-wrist control remain highly sensitive to robotic assistance but undergo somewhat smaller absolute changes in coherence.

The anterior deltoid-posterior deltoid pair showed a distinct pattern: while it exhibited the highest magnitude of change, it demonstrated significant differences in only 8 out of 9 targets. This pattern suggests that shoulder flexion-extension control shows strong sensitivity to assistance when affected, but this sensitivity may be more target-dependent compared to other muscle pairs, potentially reflecting the directional specificity of this muscle pair's

functional role in reaching.

This differential sensitivity across muscle pairs provides valuable insights into the hierarchical organization of motor control.

Scapular-pectoral coordination mechanisms (pectoralis major-posterior deltoid, middle trapezius-pectoralis major) and major joint control (biceps-triceps) showed the highest sensitivity to external assistance in terms of both consistency across targets and magnitude of change. Scapular elevation-depression control (upper-lower trapezius) and multi-joint coordination (biceps-extensor carpi ulnaris) showed universal target involvement but with smaller magnitudes. Shoulder flexion-extension control (anterior-posterior deltoid) demonstrated high magnitude changes but with less universal consistency, suggesting task-dependent modulation of assistance effects on this specific coordination pattern.

4.1.4 Neurophysiological Mechanisms and Motor Control Implications

The consistent reduction in beta-band coherence across all muscle pairs when robotic assistance was introduced suggests systematic alterations in corticospinal drive and sensorimotor integration. In unassisted movement, joint stability is achieved through coordinated muscle activity, with beta-band intermuscular coherence reflecting common neural drive to the muscles involved in the task [Farmer et al., 1993]. The observed coherence reductions indicate that this neural stabilization strategy shifts when external mechanical support is available, potentially reflecting reduced reliance on active intermuscular coupling for joint control. Notably, despite testing two distinct

assistance levels, no significant differences emerged between low and high support conditions for any muscle pair, this suggests a threshold phenomenon rather than an incremental response to the amount of support provided. The nervous system appears to categorize movement contexts categorically as either "assisted" or "unassisted" rather than processing assistance magnitude along a continuum, challenging traditional assumptions about graded motor adaptation responses.

One interpretation involves the neural mechanisms underlying alternating muscle activation during voluntary movement. Under normal conditions, agonist-antagonist muscle pairs must be precisely coordinated, with the observed reduction in beta-band coherence potentially indicating that these precise timing requirements are modified when external mechanical support provides guidance and stability. Another consideration involves sensorimotor feedback mechanisms, where the reduction in coherence under robotic assistance could suggest that external mechanical guidance reduces the demand for rapid, coordinated responsiveness.

However, it should be emphasized that while various motor control frameworks exist that might explain these findings, our coherence measurements cannot directly validate any specific theoretical model. The observed changes could result from multiple interacting factors, including altered sensory feedback, modified motor planning strategies, changes in reflex gains, or redistributed neural resources. Additionally, our coherence measurements alone cannot establish the functional significance of these changes, preventing us from determining whether the observed alterations reflect beneficial adaptations, problematic dependencies, or neutral responses to external support.

4.2 Potential clinical implications for robotic rehabilitation

These coherence reductions observed in healthy participants during short-term exposure to FLOAT assistance provide insights into how external support influences intermuscular coordination. While these findings can not be directly extrapolated to clinical populations or long-term therapeutic outcomes, they offer a preliminary understanding that may inform future investigations of robotic therapy protocols. It is important to emphasize that the present study provides mechanistic insight into motor control responses rather than direct evidence for rehabilitation efficacy. The observed coordination changes in this healthy cohort suggest that robotic assistance may influence fundamental aspects of motor control, though whether similar mechanisms operate in patient populations with neurological impairments remains to be determined. These findings warrant further investigation in clinical contexts to establish their therapeutic relevance.

4.2.1 Potential Therapeutic Benefits and Applications

The observed reduction in beta-band intermuscular coherence under robotic assistance may suggest that external mechanical support modulates neural synchronization between muscle pairs. Similar modulation of intermuscular coherence has been reported when task constraints were altered through external control interfaces during dynamic movement [He et al., 2024]. Al-

though the present findings were obtained in healthy participants, such changes in intermuscular coupling may have potential relevance for rehabilitation settings, where external assistance is used to shape motor coordination strategies.

Despite testing two distinct levels of robotic support, no significant differences were found between the low and high assistance conditions for any muscle pair. This observation in healthy participants may suggest that even minimal levels of robotic support could be sufficient to achieve these neural coordination changes, though whether this pattern translates to therapeutic contexts requires empirical validation in patient populations.

The differential sensitivity observed across muscle pairs provides important targeting information that could potentially inform future clinical investigations. Scapular-pectoral and primary joint coordination mechanisms demonstrated the most consistent responses to assistance across reaching targets, suggesting that robotic devices may be particularly effective in modifying proximal shoulder control and elbow coordination strategies. The observed variations in sensitivity across muscle pairs indicate that rehabilitation interventions might achieve optimal results when targeting movements that engage scapular stabilization and shoulder adduction-extension control.

For patients with abnormal synergistic patterns or excessive co-contraction, the observed reduction in neural synchronization between muscle pairs could potentially provide therapeutic benefits. Abnormally high intermuscular coherence has been associated with impaired selective muscle control in neurological conditions, where patients struggle to activate individual muscles independently. The ability of robotic assistance to reduce

neural synchronization requirements might help patients access more selective activation patterns, though this hypothesis requires clinical validation.

4.2.2 Design Considerations and Safety

Dependency Considerations: While reduced coordination demands may offer therapeutic benefits, observed changes also raise concerns about the possible dependency on external support and the ability to maintain motor improvements when assistance is removed[Reinkensmeyer et al., 2009]. The consistent reduction in intermuscular coherence across all participants suggests that the nervous system rapidly modifies its control strategies in the presence of robotic assistance, potentially leading to a reliance on external stabilization mechanisms. Whether patients can effectively transition back to unassisted movement after extended periods of robotic training remains an important clinical consideration.

Protocol Design Implications: The finding that no statistically significant differences in coordination changes were detected between low and high assistance levels presents opportunities and challenges for therapeutic applications. While the absence of statistically significant differences in IMC between low and high assistance may suggest potential efficiency in therapeutic protocols, the lack of statistical significance should not be interpreted as evidence of equivalence. Questions remain about the optimal level of support to promote motor recovery. If coordination strategies respond categorically to the presence versus absence of assistance, with less sensitivity to assistance magnitude within the tested range, gradually reducing assistance levels may not provide the progressive challenge typically assumed to be necessary for

motor learning and recovery[Patton et al., 2006].

Monitoring Requirements: The systematic nature of coordination changes observed in healthy individuals requires careful monitoring in clinical applications[Marchal-Crespo and Reinkensmeyer, 2009]. The development of protocols that can distinguish between beneficial neural adaptations and potentially problematic alterations in motor control will be essential for the safe implementation of robotic rehabilitation technologies.

Safety Considerations: The pattern of coordination changes evident in healthy individuals necessitates important safety considerations for clinical applications. While reduced intermuscular coherence may represent beneficial adaptation in certain scenarios, it could potentially indicate problematic alterations in motor control strategies in others. Understanding the relationship between changes in intermuscular coherence and functional motor outcomes will be essential for the safe implementation of robotic rehabilitation technologies.

The preservation of some coordination even under maximal assistance conditions provides some reassurance that fundamental motor control mechanisms are not entirely disrupted. However, the clinical significance of this residual coordination remains unclear and requires further investigation.

However, the relationship between changes in intermuscular coherence and functional motor outcomes requires empirical validation through clinical studies[Hornby et al., 2008; Mehrholz et al., 2007]. While these neural coordination changes are observable, their translation into improved movement quality, reduced disability, or enhanced activities of daily living remains to be established through controlled clinical trials that incorporate functional

measures and patient-reported outcomes.

4.3 Limitations and future directions

The present study provides valuable insights into how robotic assistance provided by the FLOAT exoskeleton affects intermuscular coordination during reaching movements, yet several methodological and conceptual limitations must be acknowledged. These limitations, while not undermining the validity of the findings, highlight important considerations for interpreting the results and suggest directions for future research.

4.3.1 Study Population and Generalizability

The investigation was conducted exclusively with healthy adults (mean age: 31±6 years), which represents a significant limitation for clinical translation. While this population allowed for examination of fundamental motor control responses to robotic assistance without confounding factors related to neurological impairment, the findings cannot be directly extrapolated to patient populations who would ultimately benefit from robotic rehabilitation technologies. Individuals with stroke, spinal cord injury, or other neuromotor disorders may exhibit fundamentally different responses to external assistance due to altered neural pathways, impaired sensorimotor integration, or compensatory movement strategies.

The relatively young age of participants also limits generalizability to older adults, who represent a significant population of potential users for robotic rehabilitation devices. Age-related changes in motor control, muscle

strength, and neural plasticity could significantly influence how intermuscular coordination responds to external support. Future studies should investigate these coherence changes across different age groups and, more importantly, in patient populations with varying types and severities of motor impairments.

4.3.2 Experimental Design and Measurement Limitations

Several aspects of the experimental design restrict the interpretation and scope of the findings. The relatively small sample size (n = 20) limits the statistical power for detecting subtle effects and reduces generalizability. The single-session design provides only a snapshot of immediate responses to FLOAT assistance, without providing information about adaptation over time or the persistence of coordination changes.

An important limitation concerns the specificity of findings to the FLOAT exoskeleton. The results are specific to the particular characteristics of FLOAT, including its mechanical design, degrees of freedom, and method of providing gravitational support. Different robotic devices with varying kinematic structures, control strategies, or assistance paradigms may influence intermuscular coordination in fundamentally different ways. Therefore, these findings can not be extrapolated to other forms of external mechanical support or different robotic rehabilitation devices without empirical validation. Future studies should compare coherence changes across multiple robotic platforms to identify device-specific versus general effects of robotic assistance.

The clinical implications of altered coordination patterns raise impor-

tant questions about treatment outcomes and motor independence. Future research should investigate whether patients can easily transition back to normal coordination patterns when assistance is removed, and whether prolonged exposure to robotic assistance affects the ability to perform unassisted movements effectively.

4.3.3 Task Complexity and Real-World Relevance

The standardized reaching task, while appropriate for controlled investigation of motor coordination, represents a simplified version of the movements of the upper limbs in the real world. Daily activities typically involve more complex, multi-step movements with varying loads, obstacles, and precision requirements that were not captured in the experimental protocol. The touch panel targets were positioned within a limited workspace, potentially missing coordination changes that might occur during movements requiring a greater range of motion or different postural demands.

4.3.4 Measurement Scope and Multimodal Assessment

Intermuscular coherence, while providing valuable information on neural coordination, represents only one aspect of motor control. The present study focused exclusively on coherence analysis and did not include assessment of EMG amplitude, movement kinematics, or force production. This narrow analytical focus means that important complementary information about muscle activation levels, movement quality, trajectory efficiency, and force

modulation strategies was not captured. The EMG analysis was limited to six muscle pairs, which may not capture the full complexity of upper limb coordination, involving numerous muscles that act synergistically. Surface EMG recordings are susceptible to crosstalk between adjacent muscles and may not accurately represent deep muscle activity. Additionally, the fixed preprocessing parameters (a 10Hz high-pass filter and 512ms analysis windows) represent methodological choices that may influence coherence estimates. The relationship between changes in coherence and functional movement outcomes remains unclear in the present analysis. Future studies should incorporate complementary measures, including EMG amplitude analysis to assess muscle activation levels, kinematic analysis to evaluate movement quality and efficiency, force measurements to characterize interaction dynamics, and clinical outcome measures to establish functional relevance. The development of clinical monitoring protocols that can assess coordination changes during therapy sessions represents an important research priority, though the technical requirements and practical feasibility of implementing such monitoring systems in clinical settings require substantial development and validation.

Conclusion

This investigation of intermuscular coherence in 20 healthy young adults during robot-assisted reaching movements has revealed systematic and consistent alterations in neuromuscular coordination patterns across all examined muscle pairs. The general reduction in beta-band coherence when robotic assistance was provided, combined with the finding that these effects remained consistent regardless of assistance magnitude, provides important insights into how the nervous system responds to external mechanical support during voluntary movement.

The findings demonstrate that robotic assistance fundamentally modifies intermuscular coordination strategies, with all six muscle pairs examined showing significant coherence reductions compared to unassisted movement. The absence of statistically significant differences detected between low and high assistance levels may suggest that the motor control system responds categorically to the presence of external support rather than scaling responses to the magnitude of assistance within the tested range. However, this finding should not be interpreted as definitive evidence of a categorical response, as the lack of statistical significance does not confirm equivalence between conditions. This observed pattern raises questions about traditional assump-

tions regarding magnitude-dependent relationships in motor adaptation and has important implications for the design of rehabilitation protocols.

While these coordination changes provide valuable insights into human-robot interaction, their clinical significance remains to be established. The systematic nature of the observed effects suggests that they represent fundamental properties of motor control adaptation rather than measurement artifacts or individual strategies. However, whether these changes reflect beneficial modifications, neutral adaptations, or potentially problematic dependencies cannot be determined without long-term studies incorporating functional outcome measures.

The potential clinical implication of this work requires careful consideration of both opportunities and risks. While reduced neural synchronization requirements might offer therapeutic benefits for patients with abnormal co-contraction patterns or impaired selective muscle control, concerns about dependency development and transfer to unassisted movement must be addressed through comprehensive clinical trials. The development of evidence-based protocols that optimize therapeutic benefits while ensuring safe transition to independent function represents a critical priority for future research.

In conclusion, this study establishes that robotic assistance provided with FLOAT consistently and systematically alters fundamental aspects of intermuscular coordination during reaching movements. These findings may provide a foundation for understanding human-robot interaction in rehabilitation contexts, although additional research is needed to translate these insights into effective clinical interventions that promote motor recovery while maintaining patient safety and functional independence.

Bibliography

S. Balasubramanian, R. Colombo, I. Sterpi, V. Sanguineti, and E. Burdet. Robotic assessment of upper limb motor function after stroke. *American Journal of Physical Medicine & Rehabilitation*, 91(11 Suppl 3):S255–S269, Nov 2012. doi: 10.1097/PHM.0b013e31826bcdc1.

S. Buccelli, F. Tessari, F. Fanin, L. De Guglielmo, G. Capitta, C. Piezzo, A. Bruschi, F. Van Son, S. Scarpetta, A. Succi, et al. A gravity-compensated upper-limb exoskeleton for functional rehabilitation of the shoulder complex. *Applied Sciences*, 12(7):3364, 2022. doi: 10.3390/app12073364.

F. J. Carod-Artal, M. S. Medeiros, T. A. Horan, and L. W. Braga. Predictive factors of functional gain in long-term stroke survivors admitted to a rehabilitation programme. *Brain Injury*, 19(9):667–673, Aug 2005. doi: 10.1080/02699050400013626.

Y. T. Chen, S. Li, E. Magat, P. Zhou, and S. Li. Motor overflow and spasticity in chronic stroke share a common pathophysiological process: Analysis of within-limb and between-limb emg-emg coherence. *Frontiers in Neurology*, 9:795, Oct 2018. doi: 10.3389/fneur.2018.00795.

S. L. Crichton, B. D. Bray, C. McKevitt, A. G. Rudd, and C. D. Wolfe. Patient outcomes up to 15 years after stroke: survival, disability, quality of life, cognition and mental health. *Journal of Neurology, Neurosurgery & Psychiatry*, 87(10):1091–1098, Oct 2016. doi: 10.1136/jnnp-2016-313361.

D. Farina, N. Jiang, H. Rehbaum, A. Holobar, B. Graimann, H. Dietl, and O. C. Aszmann. The extraction of neural information from the surface emg for the control of upper-limb prostheses: emerging avenues and challenges. *IEEE Transactions on Neural Systems and Rehabilitation Engineering*, 22 (4):797–809, Jul 2014. doi: 10.1109/TNSRE.2014.2305111.

S. F. Farmer, F. D. Bremner, D. M. Halliday, J. R. Rosenberg, and J. A. Stephens. The frequency content of common synaptic inputs to motoneurones studied during voluntary isometric contraction in man. *The Journal of Physiology*, 470:127–155, 1993. doi: 10.1113/jphysiol.1993.sp019851.

F. Garro et al. NeBULA: A Standardized Protocol for the Benchmarking of Robotic-based Upper Limb Neurorehabilitation. In *2023 Annual International Conference of the IEEE Engineering in Medicine and Biology Society (EMBC)*, pages 1–4. IEEE, 2023. doi: 10.1109/EMBC40787.2023.10340242.

GBD 2019 Stroke Collaborators. Global, regional, and national burden of stroke and its risk factors, 1990-2019: a systematic analysis for the global burden of disease study 2019. *The Lancet Neurology*, 20(10):795–820, Oct 2021. doi: 10.1016/S1474-4422(21)00252-0.

P. Grosse, M. J. Cassidy, and P. Brown. Eeg-emg, meg-emg and emg-

emg frequency analysis: physiological principles and clinical applications. *Clinical Neurophysiology*, 113(10):1523–1531, Oct 2002. doi: 10.1016/s1388-2457(02)00223-7.

M. Hakonen, H. Piitulainen, and A. Visala. Current state of digital signal processing in myoelectric interfaces and related applications. *Biomedical Signal Processing and Control*, 18:334–359, 2015.

S. M. Hatem, G. Saussez, M. Della Faille, V. Prist, X. Zhang, D. Dispa, and Y. Bleyenheuft. Rehabilitation of motor function after stroke: A multiple systematic review focused on techniques to stimulate upper extremity recovery. *Frontiers in Human Neuroscience*, 10:442, Sep 2016. doi: 10.3389/fnhum.2016.00442.

X. He, W. Sun, R. Song, and W. Xu. Wavelet coherence analysis of post-stroke intermuscular coupling modulated by myoelectric-controlled interfaces. *Bioengineering*, 11(8):802, 2024. doi: 10.3390/bioengineering11080802.

J. Y. Hogrel. Clinical applications of surface electromyography in neuromuscular disorders. *Neurophysiologie Clinique*, 35(2-3):59–71, Jul 2005. doi: 10.1016/j.neucli.2005.03.001.

T. George Hornby, Darcy D. Campbell, Joel H. Kahn, Teresa Demott, Jody L. Moore, and Hilary R. Roth. Enhanced gait-related improvements after therapist- versus robotic-assisted locomotor training in subjects with chronic stroke: a randomized controlled study. *Stroke*, 39(6):1786–1792, 2008. doi: 10.1161/STROKEAHA.107.504779.

S. R. Jaiser, M. R. Baker, and S. N. Baker. Intermuscular coherence in normal adults: Variability and changes with age. *PLoS One*, 11(2):e0149029, Feb 2016. doi: 10.1371/journal.pone.0149029.

H. S. Jørgensen, H. Nakayama, H. O. Raaschou, and T. S. Olsen. Recovery of walking function in stroke patients: the copenhagen stroke study. *Archives of Physical Medicine and Rehabilitation*, 76(1):27–32, Jan 1995. doi: 10.1016/s0003-9993(95)80038-7.

M. Kelly-Hayes, A. Beiser, C. S. Kase, A. Scaramucci, R. B. D'Agostino, and P. A. Wolf. The influence of gender and age on disability following ischemic stroke: the framingham study. *Journal of Stroke and Cerebrovascular Diseases*, 12(3):119–126, May-Jun 2003. doi: 10.1016/S1052-3057(03)00042-9.

J. W. Krakauer and J. C. Cortés. A non-task-oriented approach based on high-dose playful movement exploration for rehabilitation of the upper limb early after stroke: A proposal. *NeuroRehabilitation*, 43(1):31–40, 2018. doi: 10.3233/NRE-172411.

H. I. Krebs, N. Hogan, B. T. Volpe, M. L. Aisen, L. Edelstein, and C. Diels. Overview of clinical trials with mit-manus: a robot-aided neurorehabilitation facility. *Technology and Health Care*, 7(6):419–423, 1999.

H. I. Krebs, M. Krams, D. K. Agrafiotis, A. DiBernardo, J. C. Chavez, G. S. Littman, E. Yang, G. Byttebier, L. Dipietro, A. Rykman, K. McArthur, K. Hajjar, K. R. Lees, and B. T. Volpe. Robotic measurement of arm movements after stroke establishes biomarkers of motor recovery. *Stroke*, 45(1):200–204, Jan 2014. doi: 10.1161/STROKEAHA.113.002296.

P. Langhorne, J. Bernhardt, and G. Kwakkel. Stroke rehabilitation. *The Lancet*, 377(9778):1693–1702, May 2011. doi: 10.1016/S0140-6736(11)60325-5.

D. Leonardis, M. Barsotti, C. Loconsole, M. Solazzi, M. Troncossi, C. Mazzotti, V. P. Castelli, C. Procopio, G. Lamola, C. Chisari, M. Bergamasco, and A. Frisoli. An emg-controlled robotic hand exoskeleton for bilateral rehabilitation. *IEEE Transactions on Haptics*, 8(2):140–151, Apr-Jun 2015. doi: 10.1109/TOH.2015.2417570.

M. F. Levin and D. Piscitelli. Motor control: A conceptual framework for rehabilitation. *Motor Control*, 26(4):497–517, Jul 2022. doi: 10.1123/mc.2022-0026.

H. Liu, Y. Gao, W. Huang, R. Li, M. Houston, J. S. Benoit, J. Roh, and Y. Zhang. Inter-muscular coherence and functional coordination in the human upper extremity after stroke. *Mathematical Biosciences and Engineering*, 19(5):4506–4525, Mar 2022. doi: 10.3934/mbe.2022208.

P. Maciejasz, J. Eschweiler, K. Gerlach-Hahn, A. Jansen-Troy, and S. Leonhardt. A survey on robotic devices for upper limb rehabilitation. *Journal of NeuroEngineering and Rehabilitation*, 11:3, Jan 2014. doi: 10.1186/1743-0003-11-3.

Laura Marchal-Crespo and David J. Reinkensmeyer. Review of control strategies for robotic movement training after neurologic injury. *Journal of NeuroEngineering and Rehabilitation*, 6:20, 2009. doi: 10.1186/1743-0003-6-20.

E. L. McNicol, B. Osuagwu, and A. Vučković. Task-dependent frequency of intermuscular coherence in the presence of transcutaneous electrical spinal cord stimulation: a feasibility study. *Frontiers in Human Neuroscience*, 19:1556325, Mar 2025. doi: 10.3389/fnhum.2025.1556325.

Jan Mehrholz, Cordula Werner, Joachim Kugler, and Marcus Pohl. Electromechanical-assisted training for walking after stroke. *Cochrane Database of Systematic Reviews*, 4:CD006185, 2007. doi: 10.1002/14651858.CD006185.pub2.

R. Merletti and P. Parker, editors. *Electromyography: Physiology, Engineering, and Noninvasive Applications*. Wiley, New York, NY, USA, 2004.

J. H. Moon, J. Kim, Y. Hwang, S. Jang, and J. Kim. Novel evaluation of upper-limb motor performance after stroke based on normal reaching movement model. *Journal of NeuroEngineering and Rehabilitation*, 20(1): 66, May 2023. doi: 10.1186/s12984-023-01189-6.

B. Norrving, J. Barrick, A. Davalos, M. Dichgans, C. Cordonnier, A. Guekht, K. Kutluk, R. Mikulik, J. Wardlaw, E. Richard, D. Nabavi, C. Molina, P. M. Bath, K. S. Sunnerhagen, A. Rudd, A. Drummond, A. Planas, and V. Caso. Action plan for stroke in europe 2018–2030. *European Stroke Journal*, 3(4):309–336, 2018. doi: 10.1177/2396987318808719.

J. A. Norton. Intermuscular coherence in the presence of electrical stimulation. *Frontiers in Systems Neuroscience*, 15:647430, May 2021. doi: 10.3389/fnsys.2021.647430.

E. D. Oña, R. Cano-de la Cuerda, P. Sánchez-Herrera, C. Balaguer, and A. Jardón. A review of robotics in neurorehabilitation: Towards an automated process for upper limb. *Journal of Healthcare Engineering*, 2018: 9758939, Apr 2018. doi: 10.1155/2018/9758939.

D. Park and K. J. Cho. Development and evaluation of a soft wearable weight support device for reducing muscle fatigue on shoulder. *PLoS One*, 12(3): e0173730, Mar 2017. doi: 10.1371/journal.pone.0173730.

James L. Patton, Mary Ellen Stoykov, Mark Kovic, and Ferdinando A. Mussa-Ivaldi. Evaluation of robotic training forces that either enhance or reduce error in chronic hemiparetic stroke survivors. *Experimental Brain Research*, 168(3):368–383, 2006. doi: 10.1007/s00221-005-0097-8.

J. C. Perry, J. Rosen, and S. Burns. Upper-limb powered exoskeleton design. *IEEE/ASME Transactions on Mechatronics*, 12(4):408–417, Aug 2007. doi: 10.1109/TMECH.2007.901934.

S. Pizzamiglio, M. De Lillo, U. Naeem, H. Abdalla, and D. L. Turner. High-frequency intermuscular coherence between arm muscles during robot-mediated motor adaptation. *Frontiers in Physiology*, 7:668, 2017. doi: 10.3389/fphys.2016.00668.

T. Proietti, E. Ambrosini, A. Pedrocchi, and S. Micera. Wearable robotics for impaired upper-limb assistance and rehabilitation: State of the art and future perspectives. *IEEE Access*, 10:106117–106134, 2022. doi: 10.1109/ACCESS.2022.3210514.

David J. Reinkensmeyer, Orhan Akoner, Daniel P. Ferris, and Keith E. Gordon. Slacking by the human motor system: computational models and implications for robotic orthoses. In *Annual International Conference of the IEEE Engineering in Medicine and Biology Society*, pages 2129–2132, 2009. doi: 10.1109/IEMBS.2009.5333978.

S. Reschechtko and M. L. Latash. Stability of hand force production. ii. ascending and descending synergies. *Journal of Neurophysiology*, 120(3): 1045–1060, Sep 2018. doi: 10.1152/jn.00045.2018.

E. Scheme and K. Englehart. Electromyogram pattern recognition for control of powered upper-limb prostheses: state of the art and challenges for clinical use. *Journal of Rehabilitation Research and Development*, 48(6): 643–659, 2011. doi: 10.1682/jrrd.2010.09.0177.

M. Thorngren and B. Westling. Rehabilitation and achieved health quality after stroke. a population-based study of 258 hospitalized cases followed for one year. *Acta Neurologica Scandinavica*, 82(6):374–380, Dec 1990. doi: 10.1111/j.1600-0404.1990.tb03320.x.

United Nations Department of Economic and Social Affairs, Population Division. World population prospects 2022: Summary of results. Technical Report DESA/POP/2022/TR/NO. 3, United Nations, New York, 2022.

A. M. Valevicius, Q. A. Boser, E. B. Lavoie, G. S. Murgatroyd, P. M. Pilarski, C. S. Chapman, A. H. Vette, and J. S. Hebert. Characterization of normative hand movements during two functional upper limb tasks. *PLoS One*, 13(6):e0199549, Jun 2018. doi: 10.1371/journal.pone.0199549.

J. M. Wagner, C. E. Lang, S. A. Sahrmann, D. F. Edwards, and A. W. Dromerick. Sensorimotor impairments and reaching performance in subjects with poststroke hemiparesis during the first few months of recovery. *Physical Therapy*, 87(6):751–765, Jun 2007. doi: 10.2522/ptj.20060135.

J. Wang, D. Wu, Y. Gao, and W. Dong. Interaction learning control with movement primitives for lower limb exoskeleton. *Frontiers in Neurorobotics*, 16:1086578, Dec 2022. doi: 10.3389/fnbot.2022.1086578.

M. M. Wierzbicka, A. W. Wiegner, B. T. Shahani, and R. R. Young. Role of agonist and antagonist muscles in fast arm movements in man. *Experimental Brain Research*, 63(2):331–340, 1986. doi: 10.1007/BF00236850.

Wikipedia. Degrees of freedom problem. `https://en.wikipedia.org/wiki/Degrees_of_freedom_problem`, 2024. Accessed: September 2024.

C. J. Winstein, J. Stein, R. Arena, B. Bates, L. R. Cherney, S. C. Cramer, F. Deruyter, J. J. Eng, B. Fisher, R. L. Harvey, C. E. Lang, M. MacKay-Lyons, K. J. Ottenbacher, S. Pugh, M. J. Reeves, L. G. Richards, W. Stiers, R. D. Zorowitz, American Heart Association Stroke Council, Council on Cardiovascular and Stroke Nursing, Council on Clinical Cardiology, and Council on Quality of Care and Outcomes Research. Guidelines for adult stroke rehabilitation and recovery: A guideline for healthcare professionals from the american heart association/american stroke association. *Stroke*, 47(6):e98–e169, Jun 2016. doi: 10.1161/STR.0000000000000098.

Z. A. Wright, E. Lazzaro, K. O. Thielbar, J. L. Patton, and F. C. Huang. Robot training with vector fields based on stroke survivors' in-

dividual movement statistics. *IEEE Transactions on Neural Systems and Rehabilitation Engineering*, 26(2):307–323, Feb 2018. doi: 10.1109/TNSRE.2017.2763458.

J. Yousefi and A. Hamilton-Wright. Characterizing emg data using machine-learning tools. *Computers in Biology and Medicine*, 51:1–13, Aug 2014. doi: 10.1016/j.compbiomed.2014.04.018.

M. J. Zwarts, G. Drost, and D. F. Stegeman. Recent progress in the diagnostic use of surface emg for neurological diseases. *Journal of Electromyography and Kinesiology*, 10(5):287–291, Oct 2000. doi: 10.1016/s1050-6411(00)00020-1.

Additional and Supplementary Coherence Analyses

A.1 Supplementary Beta Band Coherence Analysis

This section presents detailed coherence plots with shaded error regions for the beta band analysis discussed in Chapter 3. While the main Results chapter utilized boxplot visualizations for statistical summary and clarity, these supplementary plots provide complete frequency-domain representations of coherence patterns across assistance conditions for all muscle pairs and targets. Each figure contains nine subplots corresponding to the nine reaching targets, with coherence plotted as a function of frequency. Median coherence values are shown as solid lines (green circles for the Free condition, blue asterisks for Low assistance, and red triangles for High assistance), while the shaded regions represent the interquartile range (IQR) computed from the aggregated dataset of 20 subjects and 10 repetitions per condition.

Visual inspection of the coherence spectra across all examined muscle

pairs revealed a consistent ordering of conditions in the beta-band frequency range (13–30 Hz). The free movement condition (green) consistently exhibited the highest coherence values, followed by low assistance (blue), with high assistance (red) showing the lowest coherence. However, the magnitude of separation between conditions and the degree of overlap varied across different muscle pairs, reflecting differential sensitivity to robotic assistance. The coherence frequency plots for each muscle pair are presented below.

Biceps Brachii — Triceps Brachii :

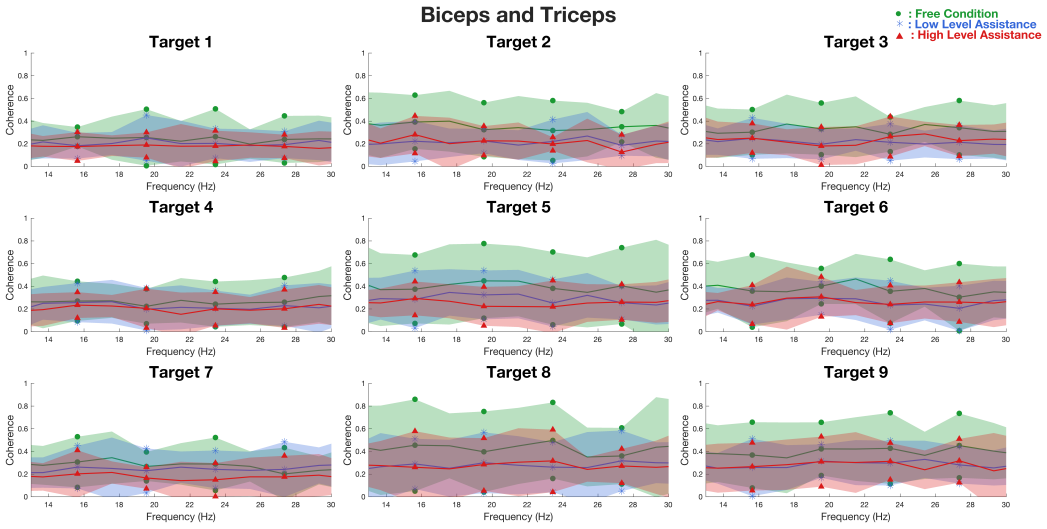

Figure A.1: Biceps and Triceps beta-band coherence frequency plot. Coherence plots show frequency-domain analysis for all reaching targets. The shaded areas represent the interquartile range (IQR) across all participants.

Anterior Deltoid — Posterior Deltoid :

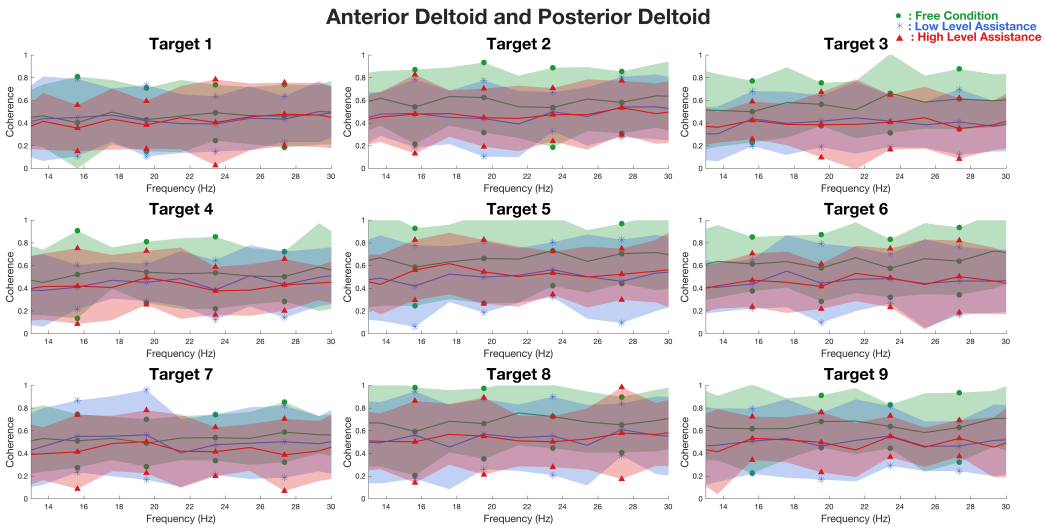

Figure A.2: Anterior and Posterior Deltoid beta-band coherence frequency plot. Coherence plots show frequency-domain analysis for all reaching targets. The shaded areas represent the interquartile range (IQR) across all participants.

Pectoralis Major — Posterior Deltoid :

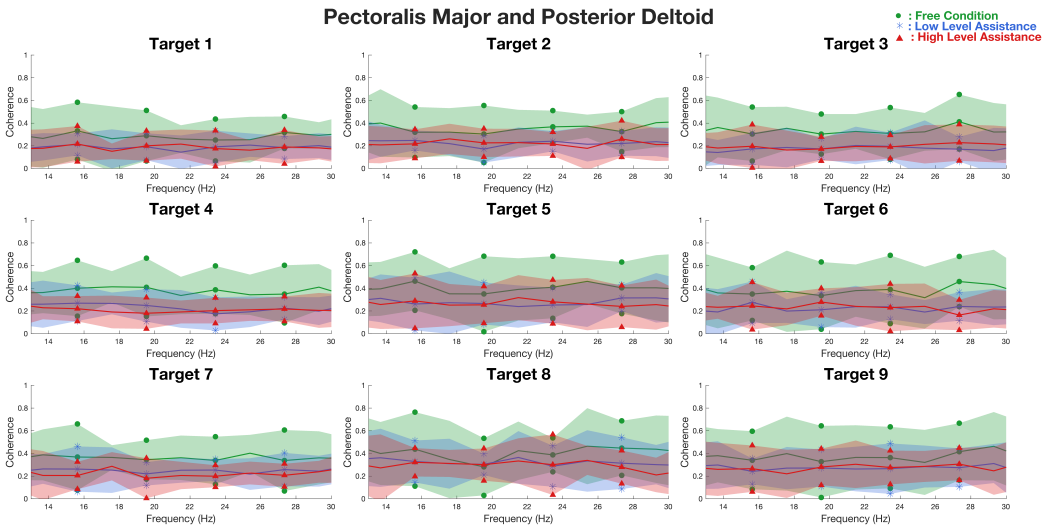

Figure A.3: Pectoralis Major — Posterior Deltoid beta-band coherence frequency plot. Coherence plots show frequency-domain analysis for all reaching targets. The shaded areas represent the interquartile range (IQR) across all participants.

Middle Trapezius — Pectoralis Major :

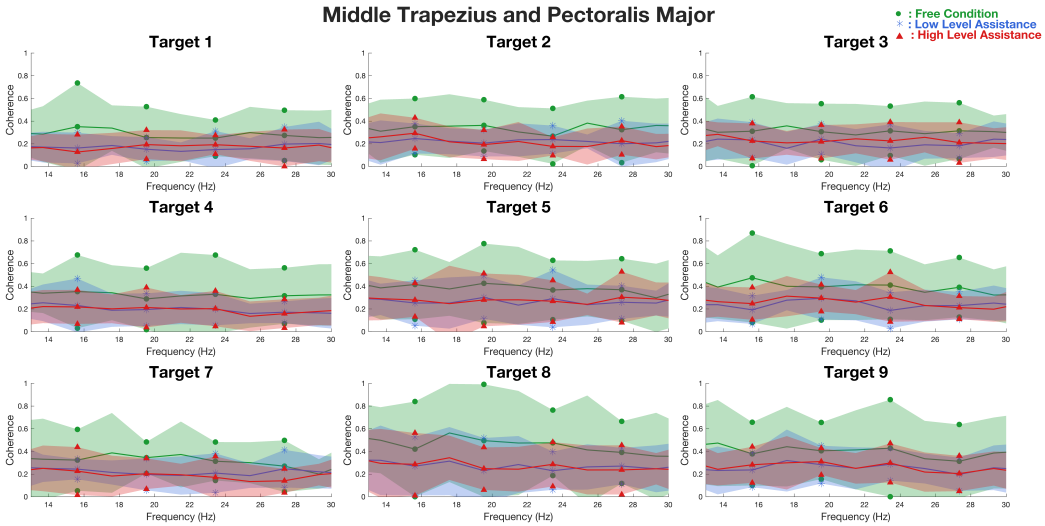

Figure A.4: Middle Trapezius — Pectoralis Major beta-band coherence frequency plot. Coherence plots show frequency-domain analysis for all reaching targets. The shaded areas represent the interquartile range (IQR) across all participants.

Upper Trapezius — Lower Trapezius :

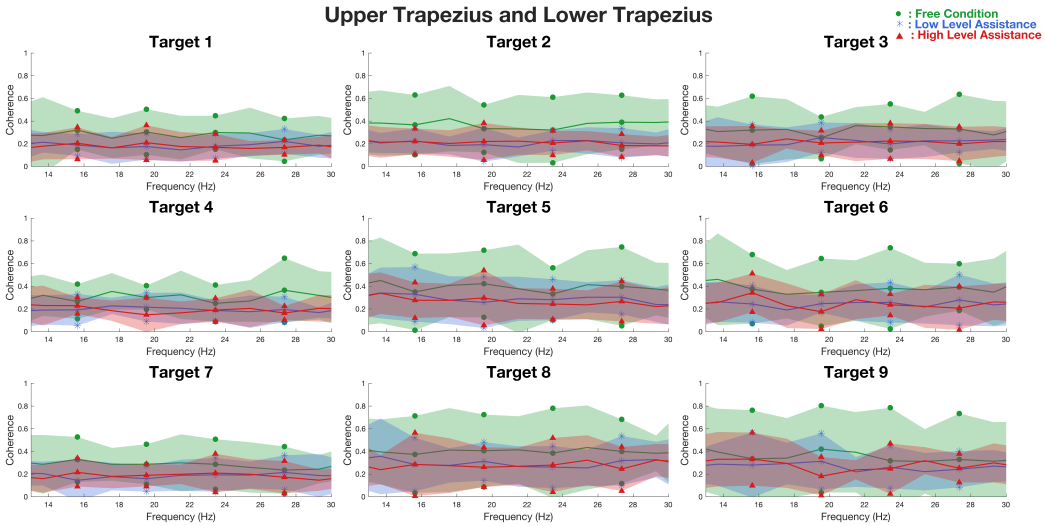

Figure A.5: Upper Trapezius — Lower Trapezius beta-band coherence frequency plot. Coherence plots show frequency-domain analysis for all reaching targets. The shaded areas represent the interquartile range (IQR) across all participants.

Extensor Carpi Ulnaris — Biceps :

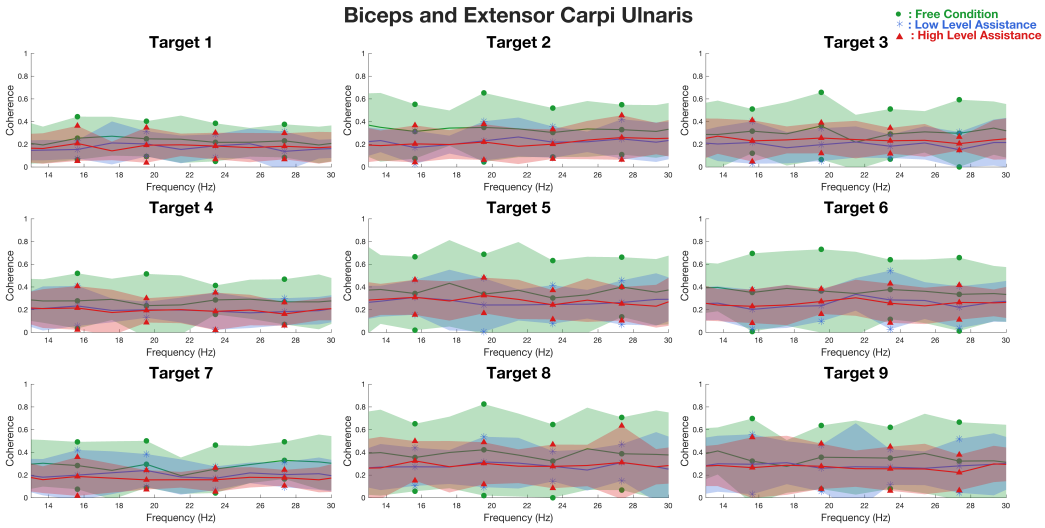

Figure A.6: Extensor Carpi Ulnaris – Biceps beta-band coherence frequency plot. Coherence plots show frequency-domain analysis for all reaching targets. The shaded areas represent the interquartile range (IQR) across all participants.

A.2 Alpha Band Coherence Analysis

Alpha band oscillations (6-12 Hz) are traditionally associated with cortical idling states, sensory inhibition, and attentional mechanisms. In the motor system, alpha band activity has been linked to cognitive aspects of motor control, including motor planning, spatial attention allocation, and

top-down regulatory processes. Unlike beta band oscillations (13-30 Hz), which reflect common neural drive and synchronization between muscles during active movement execution, alpha band coherence is thought to represent higher-order control mechanisms that remain relatively stable during motor performance.

Alpha band coherence was computed using identical analytical methods to those employed for the beta band analysis described in Chapter 2. Coherence estimation employed Welch's periodogram method with a 512-ms Hamming window, 50% overlap (256 samples), and 512-point FFT at a sampling frequency of 1000 Hz, yielding a frequency resolution of approximately 1.95 Hz.

To ensure adequate spectral sampling of the alpha band, the frequency range was defined as 5.5-13.7 Hz, extending beyond the conventional 6-12 Hz bounds. This extended range captures approximately 5 discrete frequency bins, providing sufficient spectral coverage for reliable coherence estimation and improved visualization.

Alpha band coherence (5.5-13.7 Hz) was analyzed across all six muscle pairs, nine targets, and three robotic assistance conditions to explore potential frequency-specific modulation patterns. For each muscle pair, coherence plots display median values with shaded regions representing interquartile range (IQR) across subjects for each of the nine targets. Similarly, boxplots show the distribution of median coherence values for each target, with individual subject data points connected across conditions.

Alpha band coherence exhibited the same qualitative pattern as beta band coherence (Chapter 3): Free condition showed higher coherence values

than the assisted conditions, while Low and High assistance levels remained nearly indistinguishable from each other. Specifically:

- The free condition displayed numerically higher coherence values, but with substantial overlap with the assisted conditions across all frequency points.
- The low and High assistance conditions showed nearly identical coherence distributions, replicating the pattern observed in the beta band.
- The boxplot distributions confirmed the Free $>$ Low $\approx$ High pattern across all targets.

These findings were consistent across all examined muscle pairs. The general pattern replicated the findings of the beta band (Free $>$ Low $\approx$ High) without providing additional insight or discriminatory information.

The following figures present the alpha-band coherence analysis for each muscle pair, with boxplots showing the statistical distribution across targets and conditions, and frequency-domain coherence spectra with shaded error regions representing the interquartile range across all targets.

Biceps Brachii — Triceps Brachii :

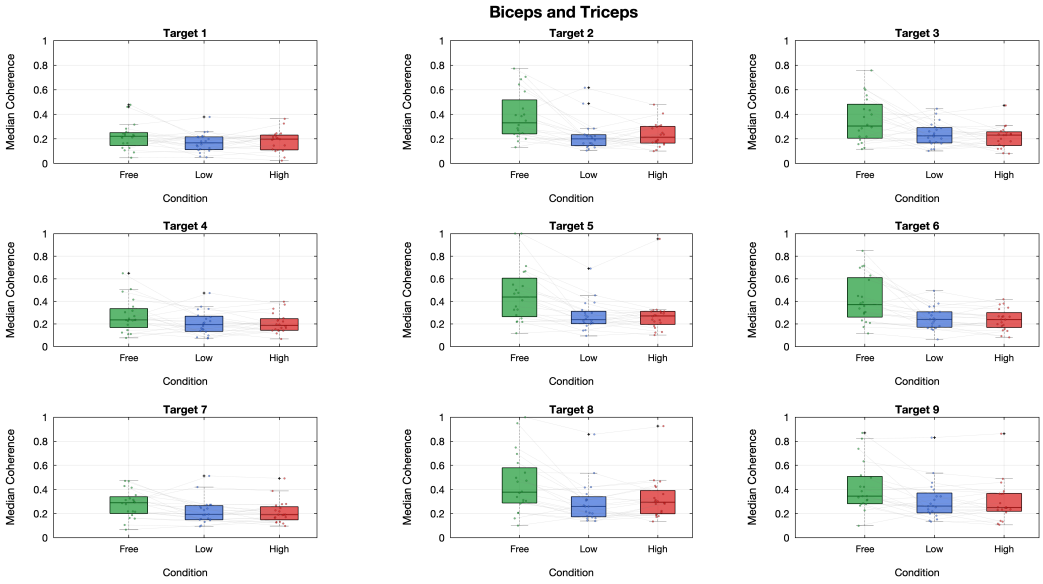

Figure A.7: Biceps — Triceps alpha-band coherence boxplot.

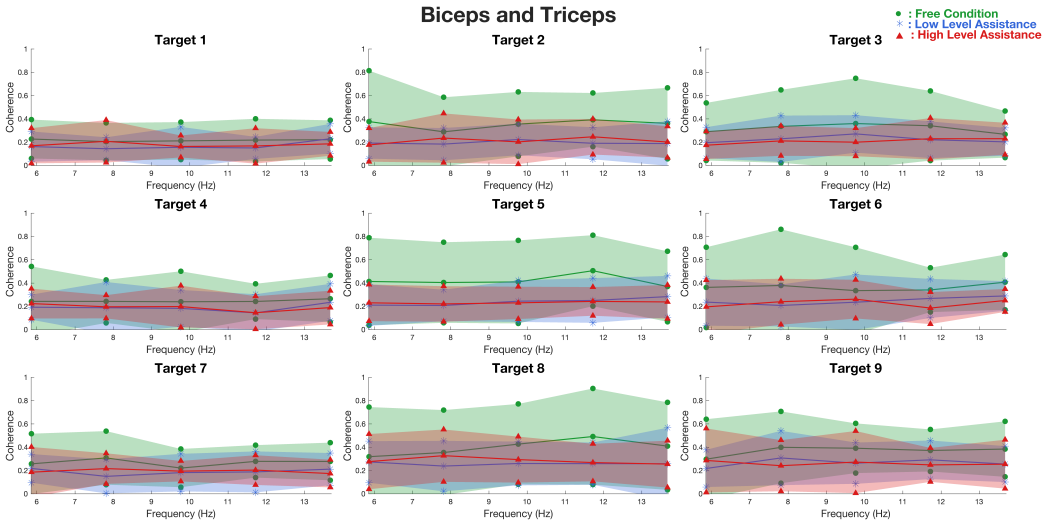

Figure A.8: Biceps — Triceps alpha-band coherence frequency spectrum.

Anterior Deltoid — Posterior Deltoid :

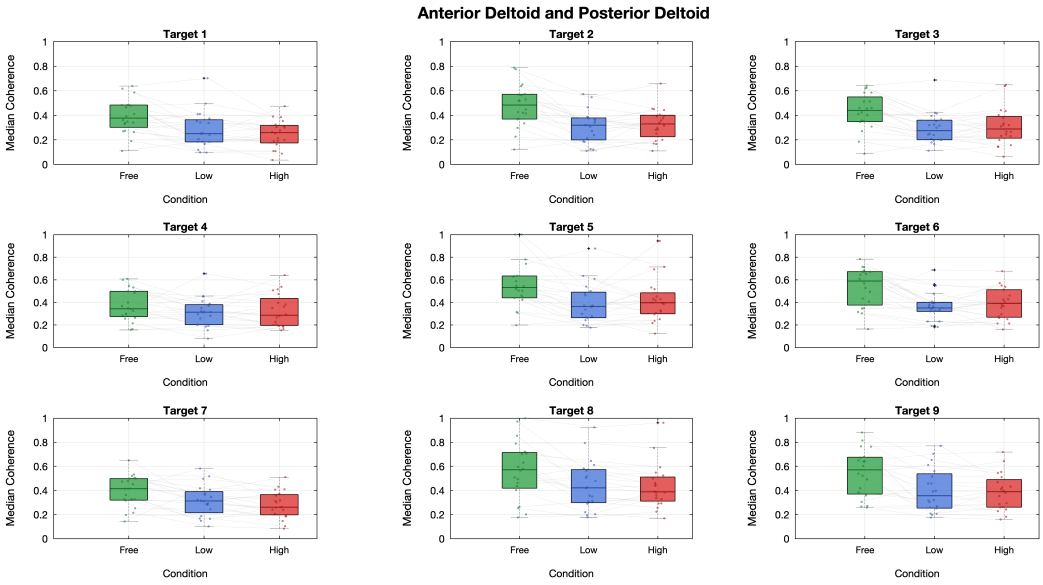

Figure A.9: Anterior — Posterior Deltoid alpha-band coherence boxplot.

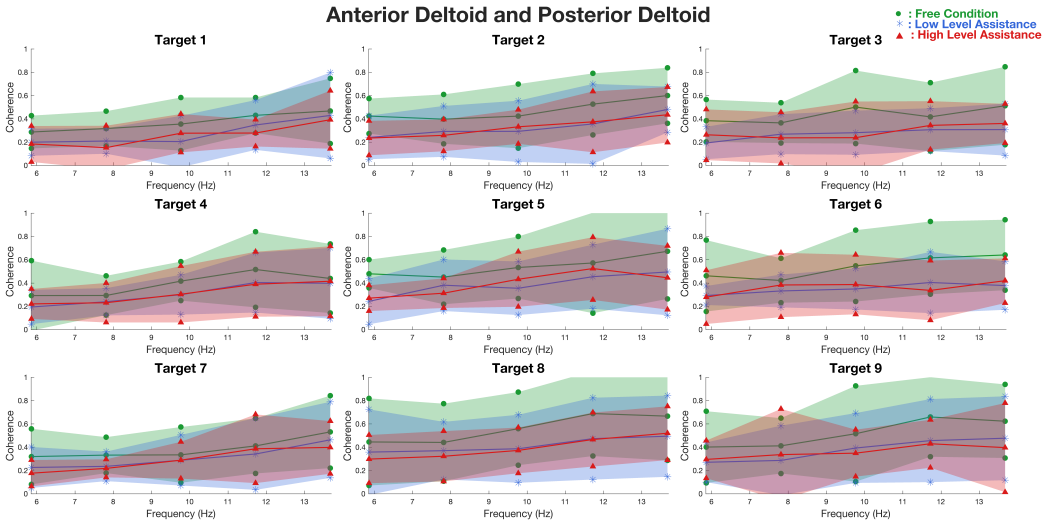

Figure A.10: Anterior — Posterior Deltoid alpha-band coherence spectrum.